

TIS Distribution Center
CSP 4-18, X7712
Syracuse, New York 13221

GENERAL ELECTRIC

MILITARY ELECTRONIC SYSTEMS OPERATION

TECHNICAL INFORMATION SERIES

Author Dr. B. A. Deresh	Subject Category Radar Height Bias Estimation	No. R82EMH3 Date June 1982
Title RADAR HEIGHT BIAS ESTIMATION FOR A GROUND- BASED RADAR USING AN AIRCRAFT ALTIMETER AS A STANDARD OF REFERENCE		
Copies Available at MESO TIS Distribution Center Box 4840 (CSP 4-18) Syracuse, New York 13221	GE Class 1	No. of Pages
	Govt Class Unclassified	83
Summary <p>Buyers of modern Air Defense radars usually specify bounds for the total root-mean-square (rms) errors of range, azimuth and height. These errors have bias and random (jitter and thermal) components which appear as summed variances. With a colocated precision track radar with known errors much smaller than the radar under test, the total rms error is established in a straightforward manner. For test sites without such a standard, the problem is more difficult. Such is the case for the majority of buyers of the GE-592 3-D Air Defense Radar. However, a standardized approach to this problem has emerged at Military Electronic Systems Operations (MESO) in which the bias and random errors are characterized separately, without the need for a colocated precision track radar. A method for making unbiased estimates of the variance of random errors has been developed by this author and a paper is currently in preparation. This paper deals entirely with the characterization of radar height bias errors.</p>		

This document contains proprietary information of the General Electric Company and is restricted to distribution and use within the General Electric Company unless designated above as GE Class 1 or unless otherwise expressly authorized in writing.

APPROVED FOR RELEASE
Approved for public release
Distribution Unlimited

Send to 82 07 23 007

GENERAL ELECTRIC COMPANY TECHNICAL INFORMATION

Within the limitations imposed by Government data export regulations and security classifications, the availability of General Electric Company technical information is regulated by the following classifications in order to safeguard proprietary information:

CLASS 1: GENERAL INFORMATION

Available to anyone on request.
Patent, legal and commercial review
required before issue.

CLASS 2: GENERAL COMPANY INFORMATION

Available to any General Electric Company
employee on request.
Available to any General Electric Subsidiary
or Licensee subject to existing agreements.
Disclosure outside General Electric Company
requires approval of originating component.

CLASS 3: LIMITED AVAILABILITY INFORMATION

Original Distribution to those individuals with
specific need for information.
Subsequent Company availability requires
originating component approval.
Disclosure outside General Electric Company
requires approval of originating component.

CLASS 4: HIGHLY RESTRICTED DISTRIBUTION

Original distribution to those individuals personally
responsible for the Company's interests in
the subject.
Copies serially numbered, assigned and recorded
by name.
Material content, and knowledge of existence,
restricted to copy holder.

GOVERNMENT SECURITY CLASSIFICATIONS, when required, take precedence in the handling of the material. Wherever not specifically disallowed, the General Electric classifications should also be included in order to obtain proper handling routines.

(5)

GENERAL ELECTRIC COMPANY
MILITARY ELECTRONIC SYSTEMS OPERATIONS
TECHNICAL INFORMATION SERIES

SECTION Engineering Operations
 UNIT Radar Systems Engineering
 MESO ACCOUNTING REFERENCE 510
 COLLABORATORS Dr. B. A. Deresh
 APPROVED R. L. Benfey TITLE Mgr., RSE LOCATION CSP 5 - C4, Syracuse, N. Y.

MINIMUM DISTRIBUTION - Government Unclassified Material (and Title Pages) in G.E. Classes 1, 2, or 3 will be the following.

<u>Copies</u>	<u>Title Page Only</u>	<u>To</u>
0	1	Legal Section, MESO (Syracuse)
0	1	Manager, Technological Planning, MESO (Syracuse)
5	6	G-E Technical Data Center (Schenectady)

MINIMUM DISTRIBUTION - Government Classified Material, Secret or Confidential in G.E. Classes 1, 2, or 3 will be the following.

1	0	Manager, Technological Planning, MESO (Syracuse)
---	---	--

ADDITIONAL DISTRIBUTION (Keep at minimum within intent of assigned G.E. Class.)

<u>COPIES</u>	<u>NAME</u>	<u>LOCATION</u>
5 (CLASS 1 ONLY)	DEFENSE DOCUMENTATION CENTER	CAMERON STATION, ALEXANDRIA, VA. 22314
1	L. I. Chasen	P. O. Box 8555 Philadelphia, Pa., 19101
1	A. A. Albanese	CSP 4-57, Syracuse, NY 13221
1	C. Arabadjis	CSP 3-16, Syracuse, NY 13221
1	R. L. Benfey	CSP 5-C4, Syracuse, NY 13221
1	C. E. Blom	CSP 5-M8, Syracuse, NY 13221
2	B. A. Deresh	CSP 5-C4, Syracuse, NY 13221
1	E. J. Gersten	CSP 5-K4, Syracuse, NY 13221
1	J. J. Gostin	CSP 4-58, Syracuse, NY 13221
1	H. L. Johndrow	CSP 5-G7, Syracuse, NY 13221
1	R. A. Loomis	CSP 5-J2, Syracuse, NY 13221
1	T. A. Matsumoto	CSP 1-20, Syracuse, NY 13221
1	D. J. Morrow	CSP 5-K7, Syracuse, NY 13221
1	J. L. Perry	CSP 5-K7, Syracuse, NY 13221
1	J. E. Phillips	CSP 5-W7, Syracuse, NY 13221
1	P. E. Postell	CSP 5-K7, Syracuse, NY 13221
1	E. J. Schroeder	CSP 5-K7, Syracuse, NY 13221
1	T. B. Shields	CSP 5-K7, Syracuse, NY 13221
1	F. V. Teillon	CSP 5-G7, Syracuse, NY 13221
1	A. E. Zebrowski	CSP 5-K7, Syracuse, NY 13221

TABLE OF CONTENTS

<u>Section</u>	<u>Title</u>	<u>Page</u>
I	INTRODUCTION	1-1/1-2
II	STATISTICAL DESCRIPTION OF RADAR ERRORS	2-1/2-2
III	ALTIMETER ERRORS	3-1
	3.1 Measurement Error	3-3
	3.2 Mode-C Encoding Error	3-3
	3.3 Atmospheric Variability	3-3
	3.4 Error Analysis	3-8
IV	RADIOSONDE	4-1
	4.1 Description and Hydrostatic Calculations	4-1
	4.2 Post-Flight Altimeter Correction Procedure	4-4
	4.3 Residual Standard Deviation of Mode-C Height Bias Error after Radiosonde Correction	4-8
V	ALTERNATIVE APPROACHES TO HEIGHT BIAS TESTING	5-1
	5.1 Fixed Height Bias Testing	5-1
	5.2 Total Mean-Square-Height Error Testing	5-1
	5.3 Error Analysis for the Fixed-Height Bias Test	5-2
	5.3.1 Definitions	5-2
	5.3.2 Variance of the Estimate	5-3
	5.3.3 Sample-to-Sample Correlation	5-5
	5.3.4 Error Models	5-7
	5.4 Statistical Risks	5-14
	5.5 Overall Test Structure	5-21
	5.5.1 Pass/Fail Criteria	5-22
	5.5.2 Pass/Fail Thresholds	5-25
	5.5.3 Test Conduct	5-30
	5.6 Error Analysis for the Mean-Square Height Error Test	5-30
	5.6.1 Definitions	5-32
	5.6.2 Variance of the Estimate	5-32
	5.6.3 Producer's Risk	5-37
	5.6.4 Pass/Fail Thresholds	5-38
	5.6.5 Buyer's Risk	5-38
	5.6.6 Buyer's Limit for C _B	5-42
	5.6.7 Buyer's Limit on MSE	5-42
VI	REFERENCES	6-1/6-2



Accession For
NTIS Grant ☒
DTIC TAB ☒
Unannounced ☐
Justification ☐
By *66-12 on file*
Distribution/
Availability Codes
Avail and/or
Special
Dist *A*

LIST OF ILLUSTRATIONS

<u>Figure</u>	<u>Title</u>	<u>Page</u>
3-1	ICAO Standard Atmosphere	3-2
3-2	Departures of Atmospheric Pressures from 1966 U. S. Standard at Different Latitudes	3-4
3-3	Coefficient of Pressure Variation vs Altitude	3-5
3-4	Range of Systematic Variability of Density Around the U. S. Standard Atmosphere, 1976	3-6
3-5	Range of Systematic Variability of Temperature Around the U. S. Standard Atmosphere, 1976	3-6
3-6	Standard Deviation of the Mode-C Height Bias Error vs Altitude	3-10
4-1	Vapor Pressure of Air vs Ambient Temperature	4-2
4-2	Height vs Range for 30 August 1979	4-6
4-3	Standard Deviation of Radiometer Computed Height Error vs Pressure - after Lenhard (Table 4-1)	4-11
4-4	Standard Deviation of Radiosonde Computed Pressure at a Specified Altitude (Inverse Hydrostatic Problem) - after Lenhard (Table 4-2)	4-12
4-5	Standard Deviation of Combined Altimeter and Radiosonde Height Error vs Height	4-14
5-1	Effective Number of Independent Legs vs Correlation with Number of Legs as a Parameter	5-6
5-2	Correlation as a Function of the Ratio of Flight Cycle Time to Bias Correlation Period	5-8
5-3	Effective Number of Independent Legs vs Ratio of Flight Cycle Time to Bias Correlation Period with Number of Legs as a Parameter	5-9
5-4	Standard Deviation of Fixed Height Bias Estimate with and without Radiosonde Correction - Effect of Correlation from Leg to Leg	5-13
5-5	Standard Deviation of Fixed Height Bias Estimate with and without Radiosonde Correction - Effect of Number of Legs	5-15
5-6	Standard Deviation of Fixed Height Bias Estimate with and without Radiosonde Correction - Effect of Altitude	5-16
5-7	Schematic Distributions of Estimation Error for Producer and Buyer Showing Risks as Shaded Areas	5-17

LIST OF ILLUSTRATIONS (CONT)

<u>Figure</u>	<u>Title</u>	<u>Page</u>
5-8	Producer's Risk vs Normalized Pass/Fail Threshold	5-19
5-9	Buyer's Risk vs Normalized Maximum Tolerable Fixed Bias Error with Normalized Pass/Fail Threshold as a Parameter	5-20
5-10	Producer's Risk per Test vs Total Number of Tests with Overall Risk of 10% and the Number of Permitted Failures as a Parameter	5-23
5-11	Buyer's Risk per Test vs Total Number of Tests with Overall Risk of 10% and the Number of Permitted Failures as a Parameter	5-24
5-12	Pass/Fail Threshold vs Range for Fixed Height Bias Error at Producer's Risks of 0.1, 1, and 10%	5-26
5-13	Pass/Fail Thresholds vs Range for 70 Subtests with Zero and 10 Permitted Subtest Failures and an Overall Risk of 10%	5-28
5-14	Maximum Tolerable Buyer's Limit of Fixed Height Bias vs Range for 70 Subtests with Zero and 10 Permitted Failures and an Overall Risk of 10%	5-29
5-15	Typical Elevation Coverage for a Height Bias Test with a Radiosonde Ascent Between 70 and 80 nmi Range	5-31
5-16	Theoretical and Experimental Probability Distributions for Chi-Square Central and Non-Central Random Variables	5-36
5-17	Pass/Fail Threshold for the Total Mean Square Height Error Test	5-39
5-18	Maximum Tolerable Buyer's Limit on Fixed Height Bias Error as Part of a Total Mean Square Height Error Test	5-43
5-19	Maximum Tolerable Buyer's Limit on Total Mean Square Height Error	5-45/5-46

LIST OF TABLES

<u>Table</u>	<u>Title</u>	<u>Page</u>
4-1	Coefficients of ICAO Pressure Model	4-5
4-2	Three Cases for Radiosonde Correction	4-7
4-3	Radiosonde Data for August 30, 1979	4-7
4-4	Three Cases After Radiosonde Correction	4-8

GLOSSARY

Hg	Mercury
ICAO	International Civil Aviation Organization
IFF	Identification Friend or Foe
kft	Kilofeet
mb	Millibars
MESO	Military Electronic Systems Operations
MSE	Mean-Square-Error
N	North
NBS	National Bureau of Standards
nmi	Nautical Mile(s)
rms	Root-Mean-Square

SECTION I

INTRODUCTION

Buyers of modern Air Defense radars usually specify bounds for the total root-mean-square (rms) errors of range, azimuth and height. These errors have bias and random (jitter and thermal) components which appear as summed variances. With a colocated precision track radar with known errors much smaller than the radar under test, the total rms error is estimated in a straightforward manner.* For test sites without such a standard, the problem is more difficult. Such is the case for the majority of buyers of the GE-592 3-D Air Defense Radar. However, a standardized approach to this problem has emerged at Military Electronic Systems Operations (MESO) in which the bias and random errors are characterized separately, without the need for a colocated precision track radar. A method of making unbiased estimates of the variance of random radar errors has been developed by this author and a paper is currently in preparation. This paper deals entirely with the characterization of radar height bias errors.

* The requirement for colocation stems from a need for accurate time registration between the two sites and to eliminate disparate environmental effects from clutter, multipath, and propagation.

SECTION II

STATISTICAL DESCRIPTION OF RADAR ERRORS

For all practical purposes, radar errors can be classified as either fixed or random. The fixed errors typically result from an error in design implementation (hardware or software) for which beam misplacement or pedestal tilt are examples. Random errors have various types of probability densities (e.g. uniform and Gaussian) and can be zero-mean or have a finite mean. A nonzero mean can result from a calibration error for instance, or simply be too costly to entirely eliminate. Often this mean may vary systematically with time. Uniform probability densities arise from sources like quantization. Gaussian densities arise from a collection of sources like equipment-induced jitter for example. From a sampling standpoint, an important consideration is the correlation time from sample to sample. Many errors are independent between samples. Such is the case for thermal and jitter errors which have a correlation time which is short compared to a revisit period. Often these errors are simply referred to as "random". But many bias errors are random as well, in that samples can be quite different and unpredictable from time to time although the time scale for which they seem constant may be quite large; hours or even days. Solar, ambient temperature, and average environmental factors (like refraction) are examples of sources of variable bias errors which are unpredictable and long term random beyond the point for which the radar designers can account for them by calibration or compensation.

SECTION III

ALTIMETER ERRORS

Height bias errors can derive from refraction, electronic, mechanical, and software sources. In the absence of a colocated precision track radar, a convenient source of a height standard is the identification friend or foe (IFF) Mode-C reply from the interrogated target aircraft. This IFF height comes from the altimeter, which is a barometric device employing an aviation standard international civil aviation organization (sometimes called the ICAO standard) atmosphere model. Unfortunately, this altimeter, while relatively precise, can be highly inaccurate particularly at high altitudes. Some discussion of this standard and its error is therefore in order.

Figure 3-1 shows the ICAO models for temperature and pressure. Below 18 kft the pilot scales the pressure model by a surface value obtained from the nearest weather station. Above 18 kft the model is uncorrected and based upon a surface pressure of 29.92 in. Hg (mercury) or 1013 mb (millibars). Often the pilot will use an ambient temperature measurement to further compensate his altimeter reading with the aid of a special slide rule. What he is actually doing is converting the pressure altitude into a corrected density altitude. First the barometer in the altimeter measures the pressure $p(H)$ at the true altitude H . An analog computer in the altimeter then enters the ICAO standard atmosphere of pressure versus altitude to find the altimeter setting $H_0(p)$. This may be an analog or digital process. Below 18 kft this setting is adjusted upwards approximately 1000 ft for every 1 in. Hg (33.857 mb) that the nearest applicable measured surface pressure exceeds the standard, i. e. 29.92 in. Hg (1013 mb). The height value shown to the pilot on the altimeter is thus

$$H_c(\text{kft}) = H_0(p) + \frac{P_{SL} - 1013.25}{36.922} - \left[\frac{P_{SL} - 1013.25}{269.503} \right]^2 \quad (3-1)$$

for barometric pressures less than 500 mb (18 kft) and just $H_0(p)$ for all altitudes greater than 18 kft (or pressures less than or equal to 500 mb). The level transmitted by Mode-C link is not corrected for surface pressure, however, and is just $H_0(p)$ at all altitudes.* In Equation (3-1), the following definitions apply:

* Except perhaps for the latest military aircraft like the F-15.

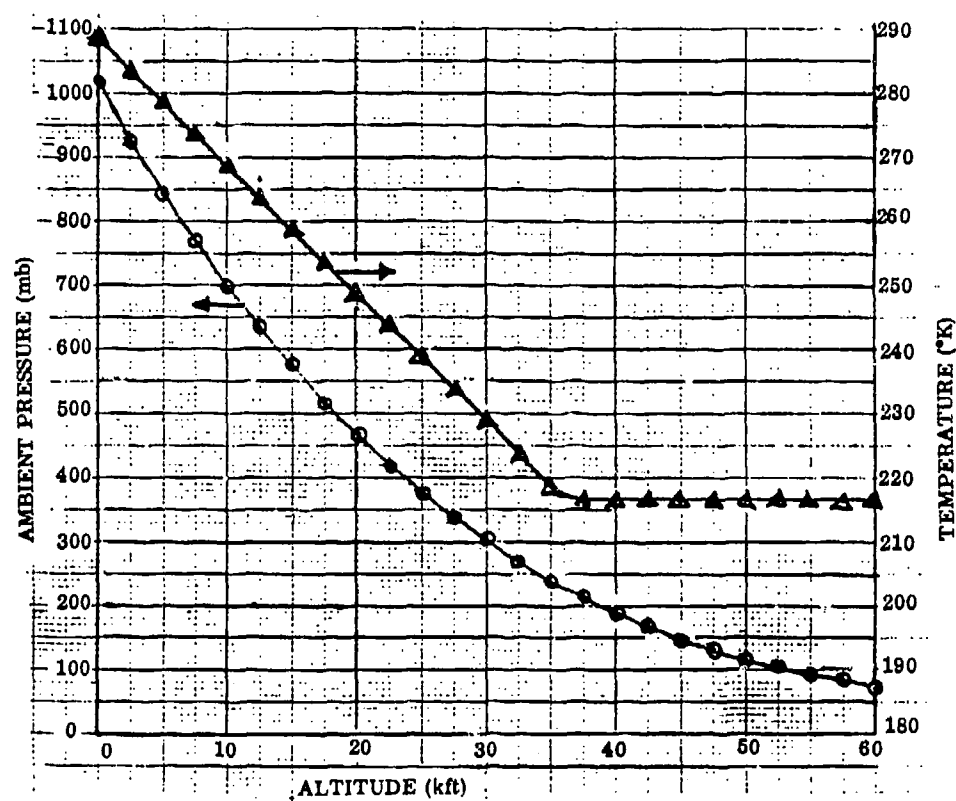


Figure 3-1. IACO Standard Atmosphere

- H_C - Mode-C height (kft)
- H_O - altimeter reading (kft)
- p - barometric pressure at true height H , (mb)
- p_{SL} - true sea level pressure (mb).

There are three principal sources of uncertainty in the Mode-C transmitted height.

1. Barometric measurement error
2. Mode-C encoding error
3. Natural atmospheric variability from the standard at all altitudes.

3.1 MEASUREMENT ERROR

The aircraft altimeter has measurement error which has both bias and random components. There doesn't seem to be any data available on the bias component, but the random (zero-mean) component seems well characterized by a standard deviation of 3 mb. The surface pressure is determined by smoothing a lot of data and has a measurement error which is negligible.

3.2 MODE-C ENCODING ERROR

The ICAO standard height is encoded onto the Mode-C transponder link with a 95th percentile error of 125 ft. This implies a standard deviation of 0.065 kft.

3.3 ATMOSPHERIC VARIABILITY

Data on the variability of pressure at sea level and at altitude is difficult to come by. Two approaches are followed here. First consider deviations from standard pressure at various north latitudes as compiled from the 1966 U.S. Standard Atmosphere (1), and shown in Figure 3-2. Presuming a uniform distribution between these limits we can infer a standard deviation and normalize by the mean. The results are plotted in Figure 3-3 as the curve connecting circles for a latitude of 60°N. Here we see zero variability at sea level, an obvious contradiction with observation. From the 1976 U.S. Standard Atmosphere (2), we have information on the variability of temperature and density shown in Figures 3-4 and 3-5. From the perfect gas law, we can derive an expression for the coefficient of variation pressure in terms of the coefficients of variation for temperature and density and the correlation between them. Thus,

U.S. STANDARD ATMOSPHERE SUPPLEMENTS, 1966

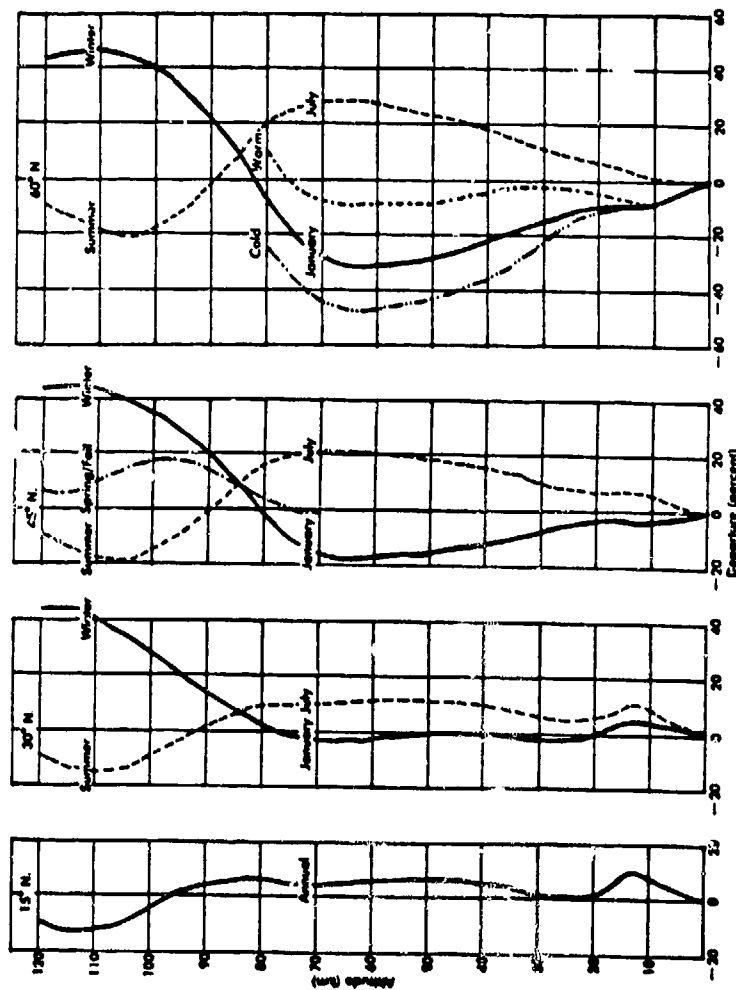


FIGURE 2.10. — Departures of Supplementary Atmospheric pressures from Standard.

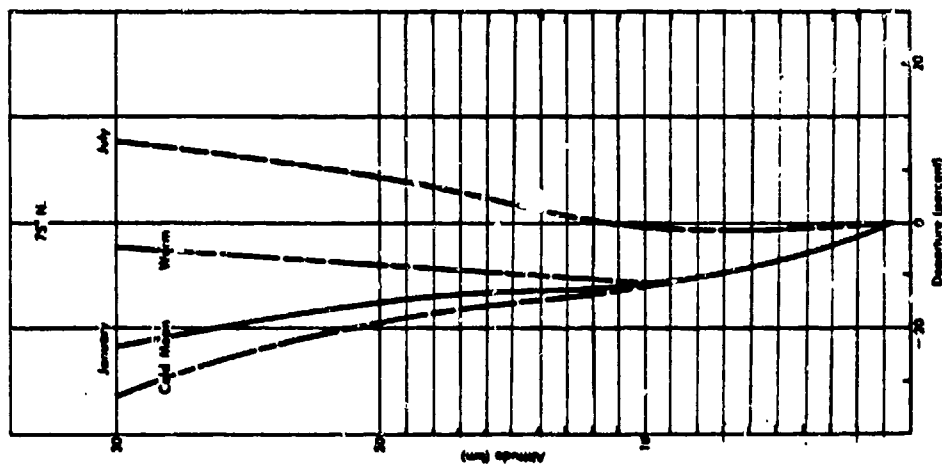


FIGURE 2.11. — Departures of 25°N. Atmospheric pressures from Standard.

Figure 3-2. Departures of Atmospheric Pressures from 1965 U. S. Standard at Different Latitudes

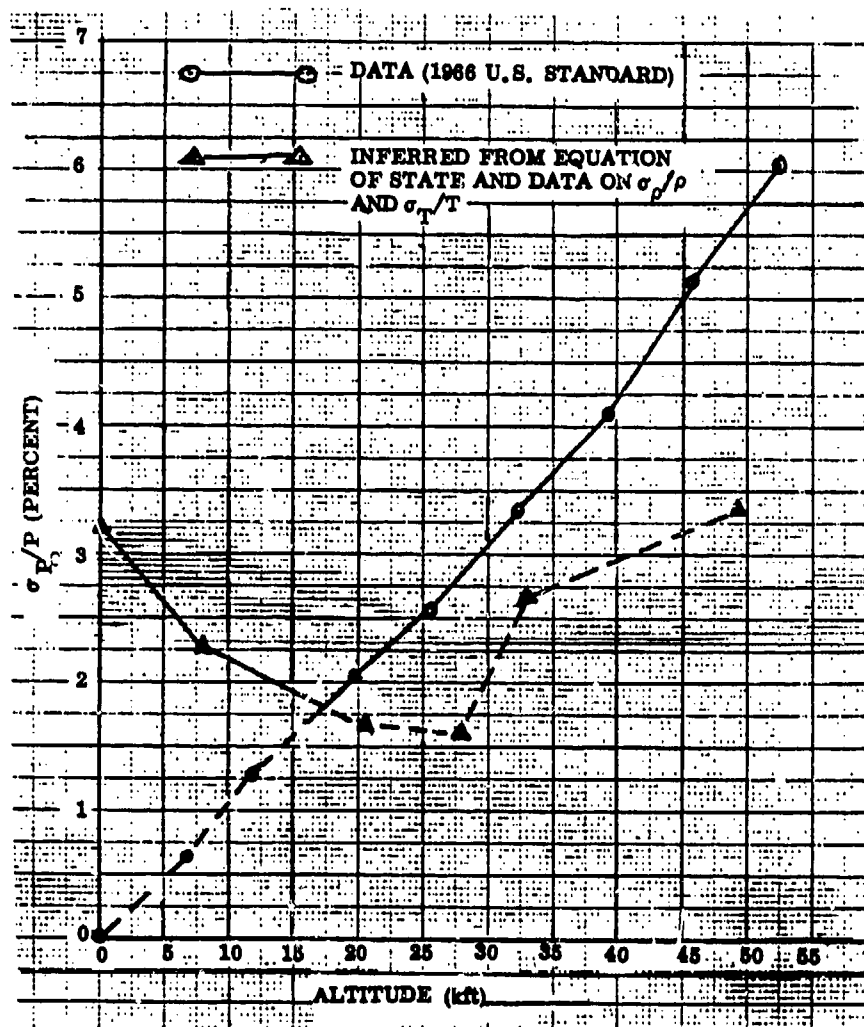


Figure 3-2. Coefficient of Pressure Variation vs Altitude

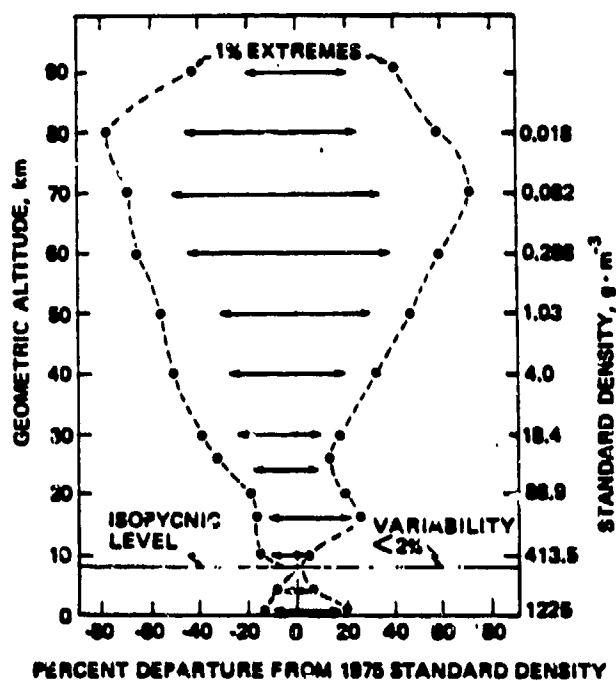


Figure 3-4. Range of Systematic Variability of Density Around the U.S. Standard Atmosphere, 1976

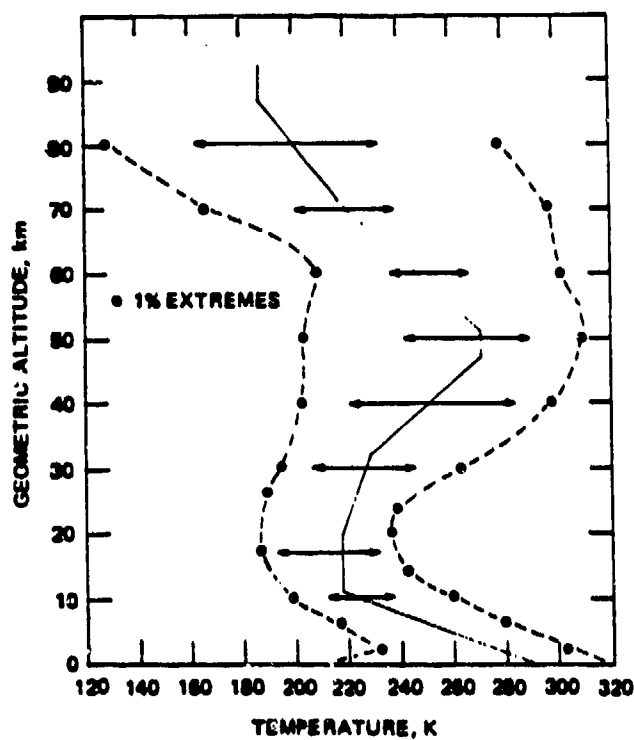


Figure 3-5. Range of Systematic Variability of Temperature Around the U.S. Standard Atmosphere, 1976.

$$\left(\frac{\hat{\sigma}_p}{p}\right)^2 = \left(\frac{\sigma_p}{p}\right)^2 + \left(\frac{\sigma_T}{T}\right)^2 + 2\rho_{pT} \left(\frac{\sigma_p}{p}\right) \left(\frac{\sigma_T}{T}\right) \quad (3-2)$$

σ_p is the inferred standard deviation of pressure (mb),

σ_p is the derived standard deviation of density (gm/cm³),

σ_T is the derived standard deviation temperature (°K),

ρ_{pT} is the correlation coefficient between measured density and temperature, i. e.

$\sigma_p T / \sigma_p \sigma_T$, and

p, ρ, T are the pressure (mb), density (gm/cm³) and temperature (°K) respectively.

Because we don't have information on the correlation between ρ and T we can assume a uniform distribution of correlations between -1 and 1, since the entire range is possible. In other words, it's just as likely that temperature increases while density decreases (increased solar heating with increasing wind velocity) as the possibility that both will increase simultaneously. An isothermal process is also possible for some measurements, corresponding to $\rho_{pT}=0$ when both the pressure and density change in proportion. Integrating Equation (3-2) over all possibilities of ρ_{pT} from -1 to 1 eliminates the last term which is equivalent by circumstance to zero correlation. Thus,

$$\frac{\hat{\sigma}_p}{p} = \sqrt{\left(\frac{\sigma_p}{p}\right)^2 + \left(\frac{\sigma_T}{T}\right)^2} \quad (3-3)$$

From Figures 3-4 and 3-5, assuming a Gaussian distribution with 1% tails we can infer standard deviations for density and temperature as input for Equation (3-3). The results are plotted in Figure 3-3 as the triangles. Since the direct data (circles) about σ_p/p is preferable but incorrect at low altitudes, we use the inferred data at low altitudes until the direct data exceeds it, in lieu of additional information. Thus we take the solid line of Figure 3-3 as definitive for the rest of the report and interpret it as the expected variability in pressure from standard at any particular altitude, place, time of day, or year (presuming ergodicity).

3.4 ERROR ANALYSIS

In this section we want to develop a reasonable model for the bias error by using the Mode-C height as an estimate of true aircraft altitude. It is a bias error in the sense that the error will not change for repeated measurements at the same altitude and range for times short compared to several hours. This error does vary as a function of target position and with times on the order of hours. For this analysis, we assume that this bias error is zero-mean Gaussian with a standard deviation that can be estimated from the data just developed. It is further assumed that the correlation between samples is on the order of 0.9 for samples taken 15-minutes apart and 0.1 for samples taken 4-hours apart. For simplicity in the analysis we can model the standard atmosphere as

$$p(\text{mb}) \cong 1033 \exp \left\{ - \frac{H^2 + 2aH}{b} \right\} \quad (3-4)$$

where

$$a \triangleq 204.8 \text{ kft}$$

and

$$b \triangleq (103.33 \text{ kft})^2.$$

From Equation (3-1), errors in the barometric altitude and encoder induce an error in the Mode-C height of

$$\delta H_c = \delta H + \delta H_{\text{enc}} \quad (3-5)$$

where,

$\delta H_{\text{enc}} \triangleq$ the transponder encoding error, and from Equation (3-4),

$$\delta H \cong \frac{\frac{b}{2a} \frac{\delta p_c}{p_c}}{1 + H/a}$$

which relates a change in altimeter pressure to a change in standard altitude in the absence of measurement error. Defining δp_m as the measurement error and δp_∞ as the variation of true pressure at altitude H.

$$\delta H_c = - \frac{\frac{b}{2a} (\delta p_\infty + \delta p_m) / p}{1 + H/a} + \delta H_{enc} .$$

Squaring and taking expectation values,

$$\sigma_{H_c}^2 = \frac{\left(\frac{b}{2a}\right)^2 \frac{\sigma_{p_\infty}^2 + \sigma_{p_m}^2}{p^2}}{(1 + H/a)^2} + \sigma_{H_{enc}}^2 \quad (3-6)$$

where from par. 3.2,

$$\sigma_{H_{enc}} = 0.065 \text{ kft.}$$

The standard deviation of altimeter error is plotted in Figure 3-6. With bias errors that have standard deviations this large, the altimeter does not appear to be a reliable standard of reference from which to estimate radar height bias errors, which are designed to be far less than those shown for the altimeter. Fortunately we can correct the altimeter after the flight by the careful use of appropriate radiosonde data.

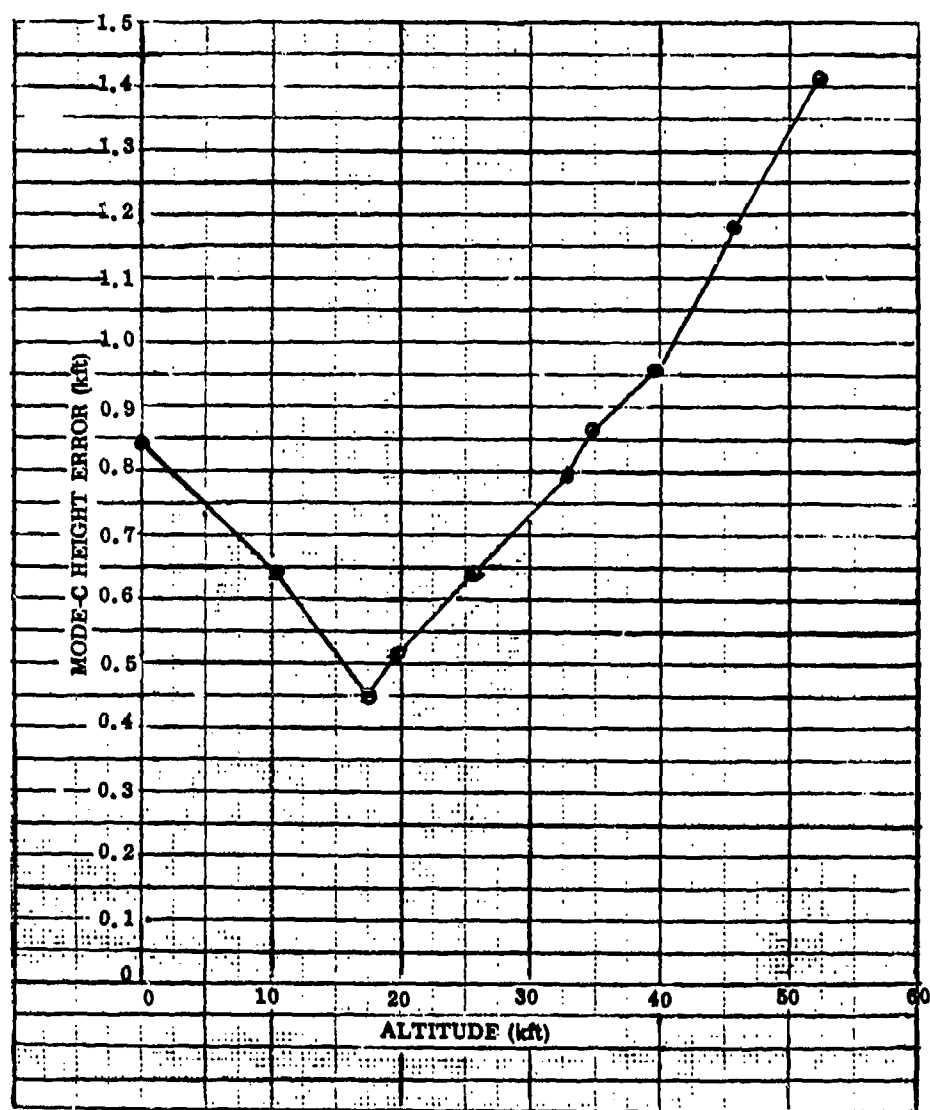


Figure 3-6. Standard Deviation of the Mode-C Height Bias Error vs Altitude

SECTION IV

RADIOSONDE

4.1 DESCRIPTION AND HYDROSTATIC CALCULATIONS

Radiosonde is a system for measuring several essential properties of the atmosphere; static pressure, temperature, relative humidity, and wind components versus altitude. The instrumentation is carried aloft by a helium balloon and the measurements are transmitted by radio down to a ground station. A tracking radar is used to estimate the wind components. The correct altitude is estimated on the ground by computer from the pressure, temperature, and relative humidity measurements by integration of the hydrostatic differential equation

$$\frac{dp}{dH} = - \frac{\alpha p}{T_v}, \quad (4-1)$$

where

p is ambient pressure (mb),
 H is altitude (kft),
 $\alpha = 10.412243$ °K/kft, and
 T_v is the virtual temperature (°K),

i. e.,

$$T_v = T(1 - 0.379 \frac{RH}{p} p_v) \quad (4-2)$$

and

T is the ambient dry-bulb temperature (°K),
 RH is the relative humidity, and
 p_v is the vapor pressure at temperature T .

The vapor pressure is the partial pressure of water vapor in the air at a given temperature T . It is an empirical function given in Figure 4-1 along with reasonable analytical models. Note that the virtual temperature reduces to the ambient temperature when the relative humidity is zero.

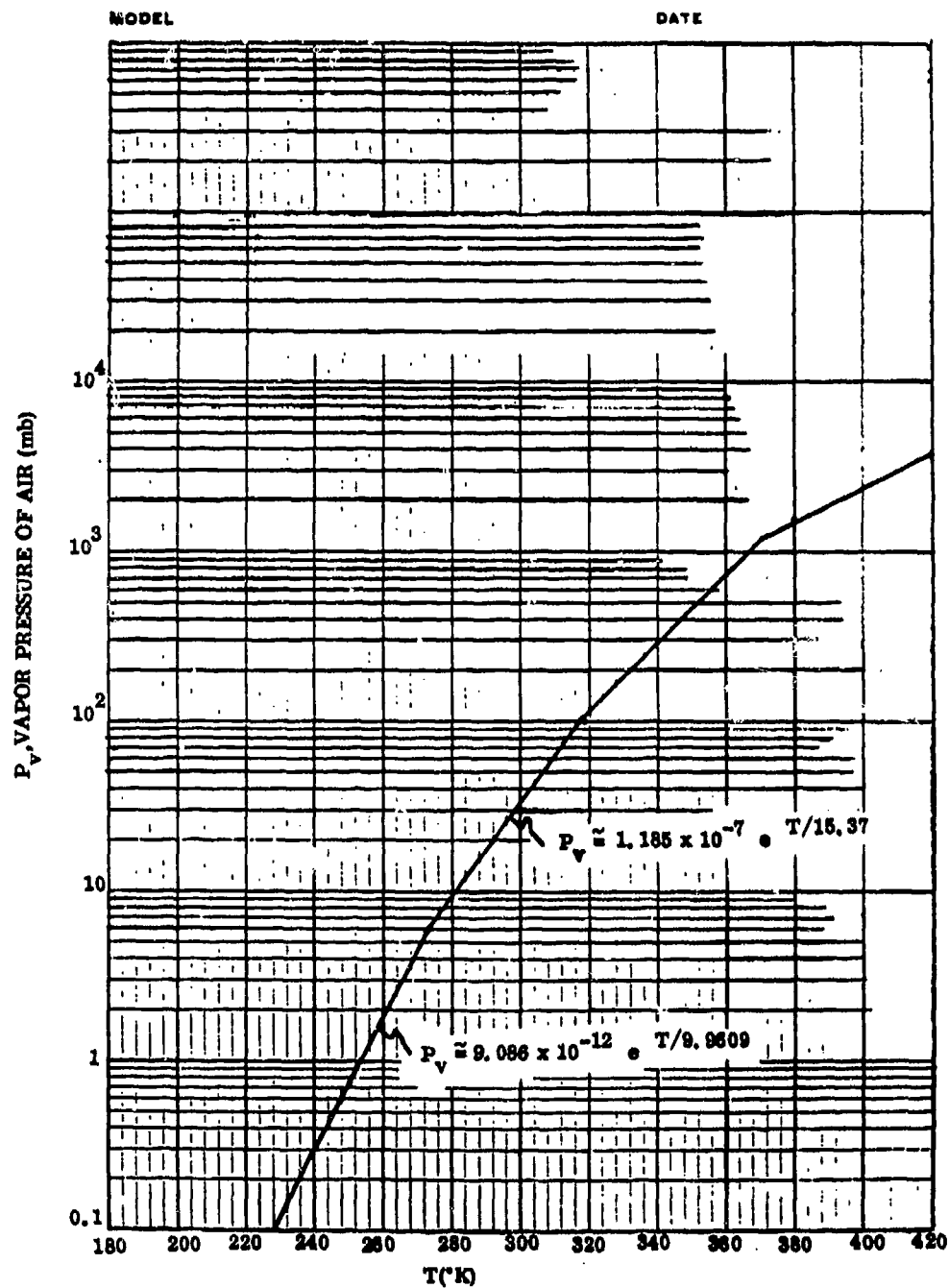


Figure 4-1. Vapor Pressure of Air vs Ambient Temperature

Two common approximations made for the temperature as a function of altitude are: (1) constant and (2) linear, within a layer defined by consecutive radiosonde transmissions.* The formulae that result are thus useful for interpolating between radiosonde reporting levels.

For a constant-temperature level, ignoring the v-subscript on virtual temperature,

$$\ln \left(\frac{p}{p_1} \right) = - \frac{\alpha}{T} \int_{H_1}^H dx$$

and

$$H = H_1 + \frac{T}{\alpha} \ln \left(\frac{p_1}{p} \right) \quad (4-3)$$

or

$$p = p_1 \exp \left[- \frac{\alpha}{T} (H - H_1) \right] \quad (4-4)$$

where the subscript 1 refers to the lower altitude report for the layer of interest.

For a variable temperature layer (assumed linear),

$$\ln \left(\frac{p}{p_1} \right) = - \alpha \int_{H_1}^H \frac{dx}{T_1 + \frac{H_2 - H_1}{T_2 - T_1} (x - H_1)}$$

and

$$H = H_1 + \left(\frac{H_2 - H_1}{T_2 - T_1} \right) T_1 \left[\left(\frac{p}{p_1} \right)^{-\frac{T_2 - T_1}{\alpha (H_2 - H_1)}} - 1 \right] \quad (4-5)$$

* Sometimes the temperature is assumed linear with pressure as a means of defining the layers. In this case the hydrostatic altitude is,

$$H = H_1 - \frac{1}{\alpha} \left\{ \frac{p - p_1}{p_2 - p_1} \cdot (T_2 - T_1) + \left[T_1 - p_1 \left(\frac{T_2 - T_1}{p_2 - p_1} \right) \right] \ln \left(\frac{p}{p_1} \right) \right\}.$$

or,

$$p = \left[1 + \frac{H - H_1}{H_2 - H_1} \left(\frac{T_2}{T_1} - 1 \right) \right]^{-\alpha \left(\frac{H_2 - H_1}{T_2 - T_1} \right)} \quad (4-6)$$

where the subscript 2 refers to the higher altitude report for the layer of interest.

4.2 POST-FLIGHT ALTIMETER CORRECTION PROCEDURE

The post-flight altimeter correction procedure consists of the following steps:

1. As a preliminary step, append virtual temperature, Equation (4-2), to the radiosonde data table.
2. Infer the altimeter barometric pressure from the ICAO standard atmosphere at the raw altitude computed in step 1.
3. Enter the radiosonde data table in the layer which would include the pressure inferred in step 2.
4. Compute the corrected altitude by interpolation according to Equations (4-3) or (4-5), depending upon whether the virtual temperature is constant or not.

Note that step 2 can be implemented either by an off-line least-squares fit to the ICAO atmosphere with an appropriate model or with a table and an appropriate interpolation algorithm. The density of the table can be traded off against accuracy according to user needs. A power series expansion good to ± 0.2 mb when using 36-bit floating point is as follows:

$$\hat{P} = \sum_{i=1}^{13} A_i (0.4H)^{i-1} \quad (4-7)$$

where \hat{P} is in millibars, H is in kilofeet, and the coefficients A_i are given in Table 4-1.

An accurate interpolation basis is as follows:

$$\hat{P} = p_k \left(\frac{p_{k+1}}{p_k} \right)^{\frac{H - h_k}{h_{k+1} - h_k}} \quad (4-8)$$

where h_k and h_{k+1} are the ICAO table entry altitudes just smaller and just larger than H respectively. The corresponding pressures in the table are p_k and p_{k+1} .

TABLE 4-1
COEFFICIENTS OF ICAO PRESSURE MODEL

1	1.0133020×10^3
2	-9.2256754×10^1
3	4.6910444
4	-1.0669557
5	3.9830776×10^{-1}
6	$-9.3698400 \times 10^{-2}$
7	1.4027070×10^{-2}
8	$-1.3812160 \times 10^{-3}$
9	9.0493196×10^{-5}
10	$-3.9030229 \times 10^{-6}$
11	1.0639916×10^{-7}
12	$-1.0613529 \times 10^{-9}$
13	$1.1322430 \times 10^{-11}$

By way of validation as well as illustration of the method consider the following example: Figure 4-2 shows actual height versus range detections for both the GE-592 radar and the IFF Mode-C link. While it is difficult for the reader to unambiguously follow the track for each sensor on the two inbound (I_2 and I_3) and two outbound legs (ϕ_3 and ϕ_4), the following table provides recorded data for three cases of interest:

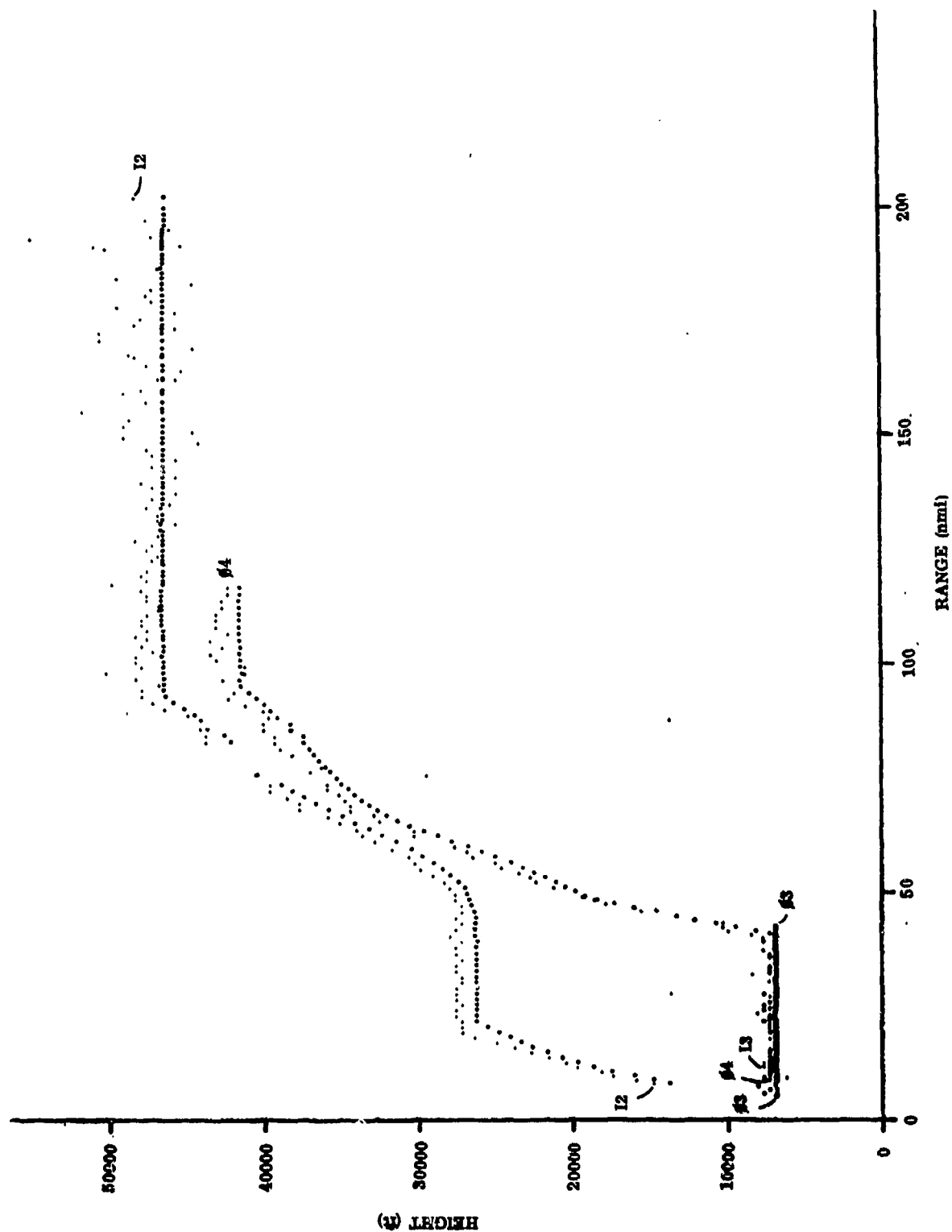


Figure 4-2. Height vs Range for 30 August 1979

TABLE 4-2

THREE CASES FOR RADIOSONDE CORRECTION

CASE	\bar{H}_R (ft)	\bar{H}_C (ft)	$\bar{H}_R - \bar{H}_C$ (ft)
1	27410	26170	+1240
2	47531	46295	+1236
3	7353	6985	+ 368

If one accepts Mode-C data without correction, one finds quite large radar bias errors, i.e., $\bar{H}_R - \bar{H}_C$. Table 4-3 summarizes the radiosonde data taken that day at two surrounding sites for the altitudes of interest.

TABLE 4-3

RADIOSONDE DATA FOR AUGUST 30, 1979

p (mb)	BUFFALO		ALBANY		AVERAGE	
	H (kft)	T_v (°K)	H (kft)	T_v (°K)	H (kft)	T_v (°K)
800	6.664	282.44	6.667	285.17	6.665	283.81
750	8.432	279.45	8.426	281.58	8.429	280.52
400	24.645	251.5	24.568	253.0	24.607	252.25
350	27.688	243.5	27.757	245.1	27.723	244.30
150	42.957	212.1	42.814	211.1	46.039	211.60
125	46.111	209.4	45.967	211.8	49.732	210.60

From Equation (4-7) the inferred ICAO pressure at the Mode-C altitude, H_C is given in Table 4-4. Using Equation (4-5) to interpolate from Table 4-3, we get H'_C , the corrected Mode-C height as given in Table 4-4. The radar error $H_R - H'_C$ has been reduced by

TABLE 4-4
THREE CASES AFTER RADIOSONDE CORRECTION

CASE	H_C (ft)	P_C (mb)	H'_C (ft)	$H_R - H'_C$ (ft)
1	26170	357.74	27277	+133
2	46295	139.13	47638	-107
3	6985	782.38	7271	+ 82

a factor of 10 at the two higher altitudes (cases 1 and 2) and by a factor of 4 for the third case. While not conclusive, this does provide compelling impetus to proceed.

4.3 RESIDUAL STANDARD DEVIATION OF MODE-C HEIGHT BIAS ERROR AFTER RADIOSONDE CORRECTION

It turns out that the radiosonde data table can be accurately interpolated without reference to the virtual temperature because virtual temperature was used to compute the hydrostatic altitudes at given pressure levels in the first place. An accurate interpolation formula which yields comparable results for the three cases considered in the previous section is,

$$\hat{H}_{nl}^c = H_1 + (H_{1+l} - H_1) \frac{\ln(\hat{P}_{nl}/p_1)}{\ln(p_{1+l}/p_1)} \quad (4-9)$$

where

\hat{H}_{nl}^c is the hydrostatically interpolated Mode-C height (kft) for the n^{th} data point and l^{th} flight leg,
 \hat{P}_{nl} is the inferred altimeter pressure (mb), logarithmically interpolated from the ICAO standard atmosphere at altitude h_{nl} .

p_i and p_{i+1} are the bracketing pressures (mb) in the radiosonde data,
 H_i and H_{i+1} are the hydrostatic altitudes (kft) corresponding to p_i and p_{i+1} , and
 h_{nl}^c is the received Mode-C height (kft).

The inferred altimeter pressure \hat{P}_{nl} is extracted from the ICAO standard atmosphere at altitude h_{nl} from,

$$\hat{P}_{nl} = P_k \left(\frac{P_{k+1}}{P_k} \right)^{\frac{h_{nl} - h_k}{h_{k+1} - h_k}} \quad (4-10)$$

where

h_k and h_{k+1} are the bracketing altitudes (kft) in the ICAO table, and
 P_k and P_{k+1} are the ICAO standard pressures (mb) which correspond to h_k and h_{k+1} .

The objective of this section is to characterize the residual error in the Mode-C height after corrections derived from applicable radiosonde data, as prescribed here and in par. 4.2. The principal sources of error in the correction procedure derive from:

1. The error derived from the measurement and use of radiosonde data, and
2. The error in retrieving the true pressure as perceived by the altimeter barometer.

From Equation (4-7) we can relate errors in radiometer pressures, p_i and p_{i+1} , and the inferred ICAO standard pressure, \hat{P}_{nl} , to the corrected Mode-C height, \hat{H}_{nl}^c . Thus,

$$\frac{\delta \hat{H}_{nl}^c}{\hat{H}_{nl}^c} = \frac{1}{\ln \left(\frac{p_{i+1}}{p_i} \right)} \left\{ \left[1 + \frac{H_{i+1}}{\hat{H}_{nl}^c} \right] \frac{\delta p_i}{p_i} - \left[\frac{H_i - H_{i+1}}{\hat{H}_{nl}^c} \right] \frac{\delta \hat{P}_{nl}}{\hat{P}_{nl}} - \left[1 - \frac{H_i}{\hat{H}_{nl}^c} \right] \frac{\delta p_{i+1}}{p_{i+1}} \right\}. \quad (4-11)$$

Now we can relate the error in the inferred ICAO standard pressure to measurement and encoder errors from Equation (4-10).

$$\frac{\delta \hat{P}_{nl}}{\hat{P}_{nl}} = \frac{\delta h_{enc}}{h_{k+1} - h_k} \ln \left(\frac{P_{k+1}}{P_k} \right) + \frac{\delta P_m}{\hat{P}_{nl}} \quad (4-12)$$

where

δh_{enc} is the encoder error ($\sigma_{h_{enc}} = 65$ ft), and

δP_m is the pressure measurement error

($\sigma_{P_m} = 3$ mb).

Lenhard in reference 3 investigated the uncertainties associated with the radiosonde procedure. Unfortunately he only characterized the standard deviation component of error and what follows is similarly limited. Here we regard his results as impacting the standard deviation of the residual error in the Mode-C height after correction by radiosonde means. His results are summarized in Figures 4-3 and 4-4 which plot the standard deviation of radiosonde computed height versus pressure and the standard deviation of radiosonde computed pressure versus height respectively. From Figure 4-4 we get δp directly versus altitude. Presuming independence between all sources of uncertainty, we combine Equations (4-11) and (4-12) and take the expectation value. Thus,

$$\begin{aligned} \left(\frac{\sigma_{H_{nl}^c}}{\hat{H}_{nl}^c} \right)^2 &= \left(\frac{1}{\ln \frac{p_{i+1}}{p_i}} \right)^2 \left\{ \left[\left(1 - \frac{H_{i+1}}{\hat{H}_{nl}^c} \right)^2 + \left(1 - \frac{H_i}{\hat{H}_{nl}^c} \right)^2 \left(\frac{p_i}{p_{i+1}} \right)^2 \right] \left(\frac{p}{p_i} \right)^2 \right. \\ &\quad \left. + \left(\frac{H_i - H_{i+1}}{\hat{H}_{nl}^c} \right)^2 \left[\left(\frac{\ln \frac{p_{k+1}}{p_k}}{h_{k+1} - h_k} \right)^2 \sigma_{h_{enc}}^2 + \left(\frac{\sigma_{P_m}}{\hat{P}_{nl}} \right)^2 \right] \right\}. \quad (4-13) \end{aligned}$$

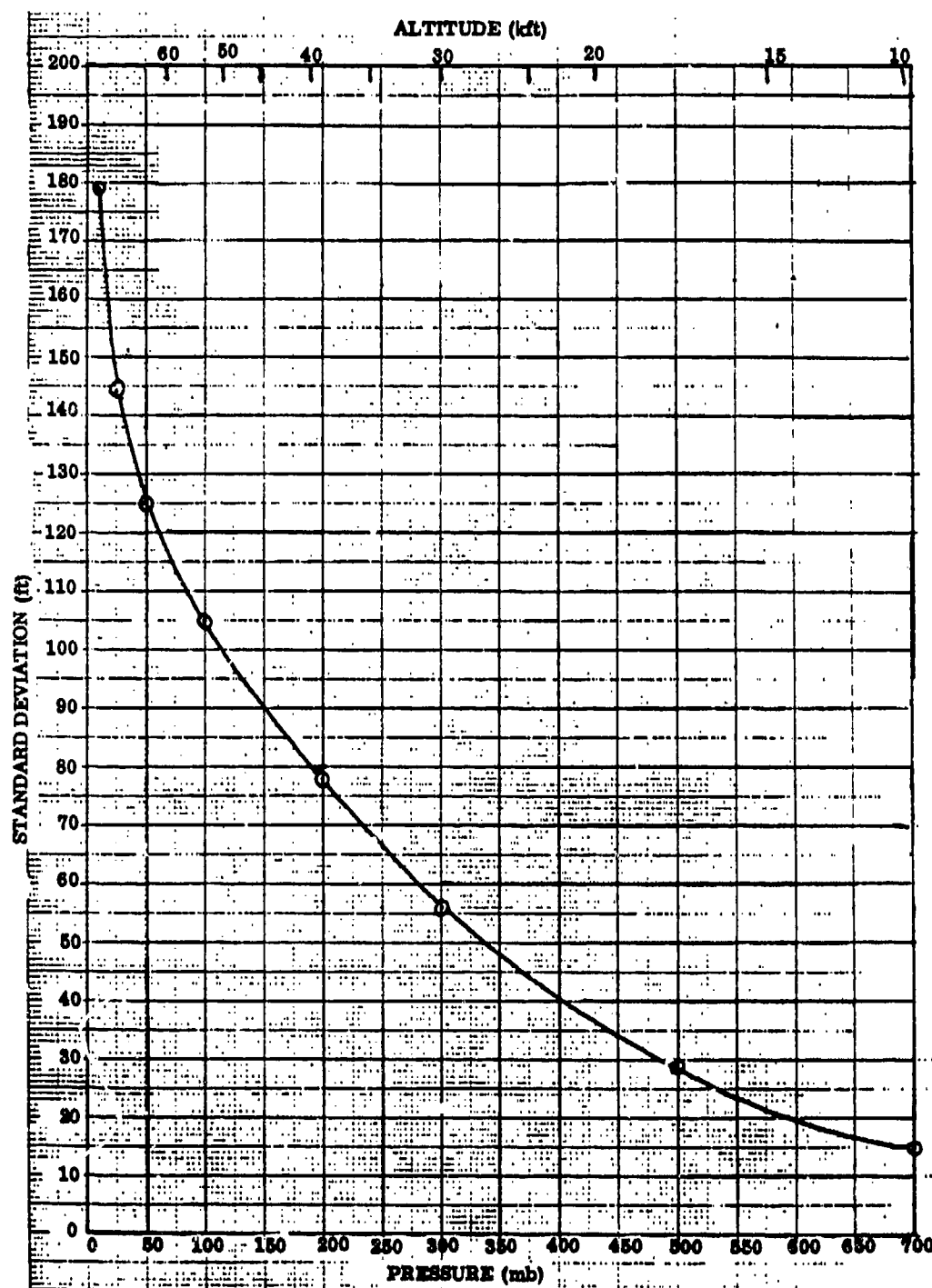


Figure 4-3. Standard Deviation of Radiometer Computed Height Error vs Pressure - after Lenhard (Table 4-1)

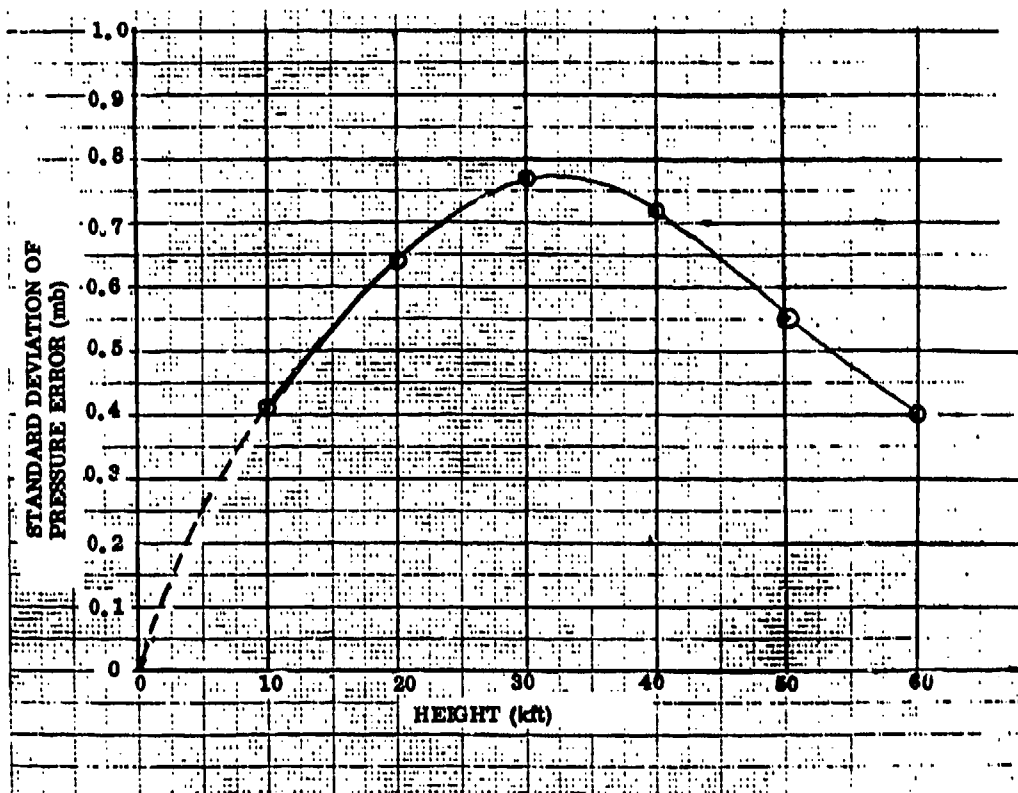


Figure 4-4. Standard Deviation of Radiosonde Computed Pressure at a Specified Altitude (Inverse Hydrostatic Problem) - after Lenhard (Table 4-2)

This error is plotted in Figure 4-5 as the upper curve. The second curve down shows the effect of encoding error while the third shows the effect of the radiosonde induced errors alone. The primary component of the error plotted in Figure 4-5 is due to the extraction of ICAO standard pressure from the Mode-C height and the attendant altimeter pressure measurement error. As such, the greatest advantage of the radiosonde correction is at altitudes below about 45 kft as can be seen by comparing the plots of Figures 3-5 and 4-5. Fortunately, this is the important region for flight tests. Nevertheless the residual error after correction at 45 kft still has a standard deviation of about 450 ft.

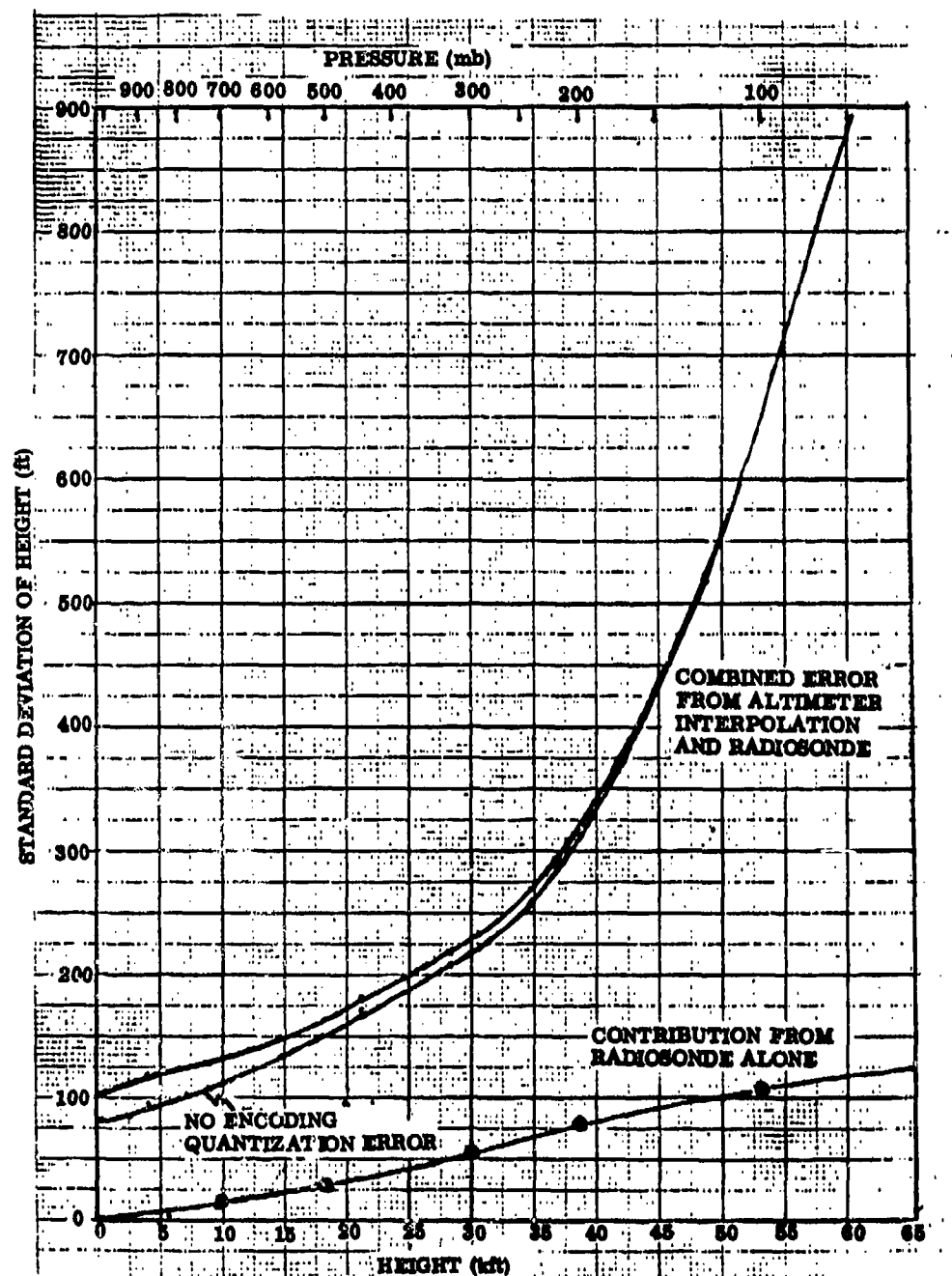


Figure 4-5. Standard Deviation of Combined Altimeter and Radiosonde Height Error vs Height

SECTION V

ALTERNATIVE APPROACHES TO HEIGHT BIAS TESTING

In the previous section, we formed the basis of an accurate height reference by introducing a method of correction to the Mode-C height. Here we expose two methods for testing radar height bias using this corrected Mode-C height reference.

5.1 FIXED HEIGHT BIAS TESTING

A hypothesis is advanced that all radar bias errors are random in the long run and zero mean. The test is designed to sample this composite long-term distribution by averaging the difference between the radar (primary) and the IFF Mode-C (secondary) over many flights of common purpose, e. g. in-the-clear at 40 kft. If radiosonde data is available, it is used to compensate and correct the secondary reference altitude on each flight leg. Pass/fail thresholds are computed from the following constraints:

1. The long-term average should be zero in the absence of fixed bias errors,
2. All bias tests flights are far apart enough in time so that independent bias samples are taken from radar equipment and atmospheric sources.
3. Producer's and buyer's risks are bounded by accommodating the appropriate sampling uncertainty.
4. If no radiosonde data is available, the expected variance of the altimeter error is included in the calculations of pass/fail thresholds.

5.2 TOTAL MEAN-SQUARE-HEIGHT ERROR TESTING

The first approach implies separate pass/fail criteria and thresholds for height bias from those used to test the variance of height accuracy. The second test approach attempts to combine the two error sources (i. e. bias and short-term random) into a test of the mean-square absolute height error.

The squared difference of primary and secondary heights is averaged on special flights designated for bias tests. Altimeter corrections are made on each flight leg in range intervals where radiosonde data is available. The sample variance is adjusted for the expected variance of atmospheric refraction biases (if refraction bias is not a responsibility of the radar producer).

The same constraints hold for each test type and pass/fail thresholds are computed from knowledge of expected theoretical performance with allowances for the limited sample size. In order to estimate the tolerance required to accommodate the uncertainty associated with a finite sample size, it is necessary to understand the statistics of the sample estimate of both the fixed height bias error and the mean-square total height error.

5.3 ERROR ANALYSIS FOR THE FIXED HEIGHT BIAS TEST

In this section we will define the error sources and introduce correlation between samples. In par. 5.4 we will then derive expressions for producer and buyer risks for test planning. In par. 5.5 we will consider this test in the context of an overall flight test where other performance measures are concurrently tested so as to introduce the concept of risk allocation. Numerical examples to tie all these ideas together are included in par. 5.6.

5.3.1 DEFINITIONS

As a prelude to the analysis, consider the definitions for a given flight test type (e. g. in-the-clear at 40 kft) and a given flight path interval. For the l^{th} flight leg and n^{th} data point, the radar (primary) errors are,

α_{ln}	the total short-term random error component of elevation angle (jitter and thermal). It is independent from point-to-point within the estimation interval and is generally considered as zero-mean Gaussian, whose variance σ_α^2 may vary systematically with range and elevation angle,
ϵ_l	the total equipment (electronic, mechanical, and software) elevation bias error which is random and independent from leg-to-leg. Its parent distribution is assumed to be zero-mean Gaussian with variance σ_ϵ^2 , which may vary systematically with range and elevation angle,
A_l	the total atmospheric elevation bias error which is random and independent from leg-to-leg. Its parent distribution (after refraction corrections) is assumed to be zero-mean Gaussian with variance σ_A^2 that varies systematically with elevation angle,
β_l	the total zero-mean Gaussian bias error which is independent from leg-to-leg. It has variance $\sigma_\beta^2 = \sigma_\epsilon^2 = \sigma_A^2$,
c	constant bias error with zero variance;
δH_{VAR}	Mode-C error without radiosonde correction in the absence of altimeter error, assumed independent from leg-to-leg and zero-mean Gaussian with variance σ_{VAR}^2 ,
\hat{c}	the height bias estimate,

H_{ln}^R	radar height measurement for the n^{th} point and l^{th} leg,
H_{ln}^C	uncorrected Mode-C height measurement for the n^{th} point and l^{th} leg,
\bar{R}	mean-range in path intervals,
δH_{ALT}	Mode-C error without radiosonde correction in the absence of atmospheric pressure variability, assumed independent from point-to-point and zero-mean Gaussian with variance σ_{ALT}^2 ,
δH_{RAD}	Mode-C height error after radiosonde correction for zero altimeter error which are assumed independent from leg-to-leg and is zero-mean Gaussian with variance σ_{RAD}^2 and
δH_{RA}	Mode-C height error after radiosonde correction in the absence of radiosonde error which is independent from point-to-point and zero-mean Gaussian with variance σ_{RA}^2 .

5.3.2 VARIANCE OF THE ESTIMATE

The height bias estimate after averaging over the N data points in the path interval and L independent flight legs is

$$\hat{c} = \frac{1}{LN} \sum_{l=1}^L \sum_{n=1}^N \left(H_{ln}^R - H_{ln}^C \right) \quad (5-1)$$

where

$$H_{ln}^R - H_{ln}^C = \bar{R} \left(\alpha_{ln} + \beta_l \right) + c + \left(\delta H_{VAR} \right)_l + \left(\delta H_{ALT} \right)_{ln} \quad (5-2)$$

if the altimeter is not corrected by radiosonde, or

$$H_{ln}^R - H_{ln}^C = \bar{R} \left(\alpha_{ln} + \beta_l \right) + c + \left(\delta H_{RA} \right)_{ln} + \left(\delta H_{RAD} \right)_l \quad (5-3)$$

if it is. Thus,

$$\begin{aligned} \hat{c} = c + \frac{1}{LN} \sum_{l=1}^L \sum_{n=1}^N \left[\bar{R} \alpha_{ln} + \left(\delta H_{RA} \right)_{ln} + \left(\delta H_{ALT} \right)_{ln} \right] \\ + \frac{1}{L} \sum_{l=1}^L \left[\bar{R} \beta_l + \left(\delta H_{VAR} \right)_l + \left(\delta H_{RAD} \right)_l \right] \end{aligned} \quad (5-4)$$

where δH_{ALT} and δH_{VAR} are ignored if radiosonde is used and the errors δH_{RA} and δH_{RAD} are ignored otherwise. Note that the estimate of c is unbiased in that

$$E(\hat{c}) = c \quad (5-5)$$

because

$$E(\alpha) = E(\beta) = E(\delta H_{VAR}) = 0$$

$$E(\delta H_{ALT}) = E(\delta H_{RAD}) = E(\delta H_{RA}) = 0$$

by definition.

The variance of the estimate is,

$$\begin{aligned} \text{VAR } \hat{c} = & \frac{1}{LN} \left[\bar{R}^2 \text{VAR } \alpha + \text{VAR}(\delta H_{RA}) + \text{VAR}(\delta H_{ALT}) \right] \\ & + \frac{1}{L} \left[\bar{R}^2 \text{VAR } \beta + \text{VAR}(\delta H_{RAD}) + \text{VAR}(\delta H_{VAR}) \right] \end{aligned} \quad (5-6)$$

where all error sources are assumed to be uncorrelated by type. The standard deviation of the unbiased estimate \hat{c} is

$$\sigma_{\hat{c}} = \sqrt{\frac{1}{LN} \left[\bar{R}^2 \sigma_{\alpha}^2 + \sigma_{RA}^2 + \sigma_{ALT}^2 \right] + \frac{1}{L} \left[\bar{R}^2 \sigma_{\beta}^2 + \sigma_{RAD}^2 + \sigma_{VAR}^2 \right]}. \quad (5-7)$$

The estimate \hat{c} is both unbiased and consistent because

$$E(\hat{c} - c) = 0 \quad (5-8)$$

and

$$\lim_{L \rightarrow \infty} \sigma_{\hat{c}} = 0. \quad (5-9)$$

5.3.3 SAMPLE-TO-SAMPLE CORRELATION

Equation (5-7) is correct only if each leg is flown far enough apart in time to independently sample all the bias errors. To gain some insight into the penalty to be paid for failure to do this consider the following informal analysis:

Let:

- T flight time of one leg,
- ΔT time between legs,
- τ total bias correlation time,
- L total number of legs,
- L_{eff} effective number of independent legs, and
- ρ correlation coefficient of bias errors.

A reasonable model for L_{eff} versus bias correlation can be constructed from the following boundary conditions:

1. For zero correlation, $L_{\text{eff}} = L$, $dL_{\text{eff}}/d\rho=0$.
2. For unity correlation, $L_{\text{eff}} = 1$, $dL_{\text{eff}}/d\rho=0$.

Without taking this quest rigorously, we can satisfy these criteria with a simple cosine function, i. e.

$$L_{\text{eff}} = \frac{L-1}{2} \cos \pi \rho + \frac{L+1}{2} \quad (5-10)$$

which is plotted in Figure 5-1 as the ratio of L_{eff}/L with L as a parameter. This plot implies that a correlation as low as 0.25 is required to achieve 90% independence between legs.

A good model for correlation as a function of the total flight cycle time $T + \Delta T$ is the Markov process. If the current bias error only depends upon the previous error (i. e. the value on the last flight leg) then we are describing a 1st order Markov process with

$$\rho = \exp \left[- \frac{T+\Delta T}{\tau} \right] . \quad (5-11)$$

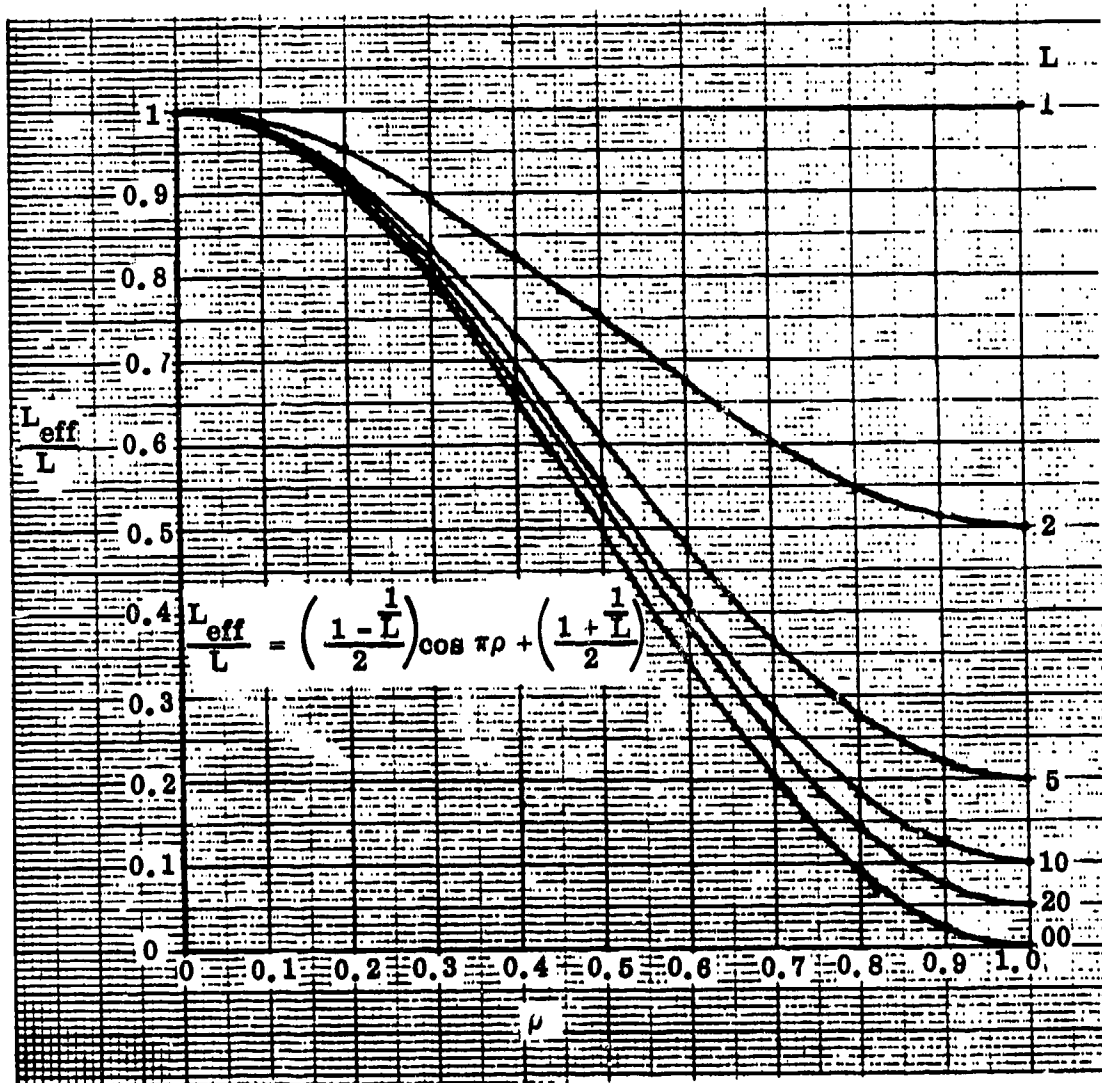


Figure 5-1. Effective Number of Independent Legs vs Correlation With Number of Legs as a Parameter

If it depends upon the last two errors (legs) then we are describing a 2nd order Markov process with

$$\rho = e^{-2.146 \left(\frac{T+\Delta T}{\tau} \right)} \left[1 + 2.146 \left(\frac{T+\Delta T}{\tau} \right) \right]. \quad (5-12)$$

These are plotted in Figure 5-2 and combined with Equation (5-10) in Figure 5-3. Here we see 90% independence can be achieved with a total flight cycle time of about 1.5τ . I have not uncovered definitive information on τ but experience with the GE-592 implies 2-8 hours. So to insure independence, legs for the bias test should be flown no more than twice a day (i. e. about 12 hours apart).

To be precise we should modify the expression for estimation error, i. e., Equation (5-7), to include leg-dependence. The first term includes errors which are independent from point-to-point so that $L_{\text{eff}} = L$. But the last two terms are bias errors so that

$$\sigma_{\hat{c}} \approx \sqrt{\frac{1}{LN} \left[\bar{R}^2 \sigma_{\alpha}^2 + \sigma_{\text{RA}}^2 + \sigma_{\text{ALT}}^2 \right] + \frac{1}{L_{\text{eff}}} \left[\bar{R}^2 \sigma_{\beta}^2 + \sigma_{\text{RAD}}^2 + \sigma_{\text{VAR}}^2 \right]}. \quad (5-13)$$

5.3.4 ERROR MODELS

To gauge the value of these ideas, we need representative models for σ_{α} and σ_{β} for a typical air defense radar (not necessarily the GE-592) without special features (e. g. multipath-defeating angle measurement techniques, SNR weighting for multiple-hits, etc.). For random errors,

$$\sigma_{\alpha}^2 = \sigma_{\alpha_J}^2 + K \left(\frac{R}{R_0} \right)^4 \quad (5-14)$$

with

$$\sigma_{\alpha_J} = \begin{cases} 0.65 \text{ mrad; } R \leq R_0 \\ 0.9 \text{ mrad; } R > R_0 \end{cases} \quad (5-15)$$

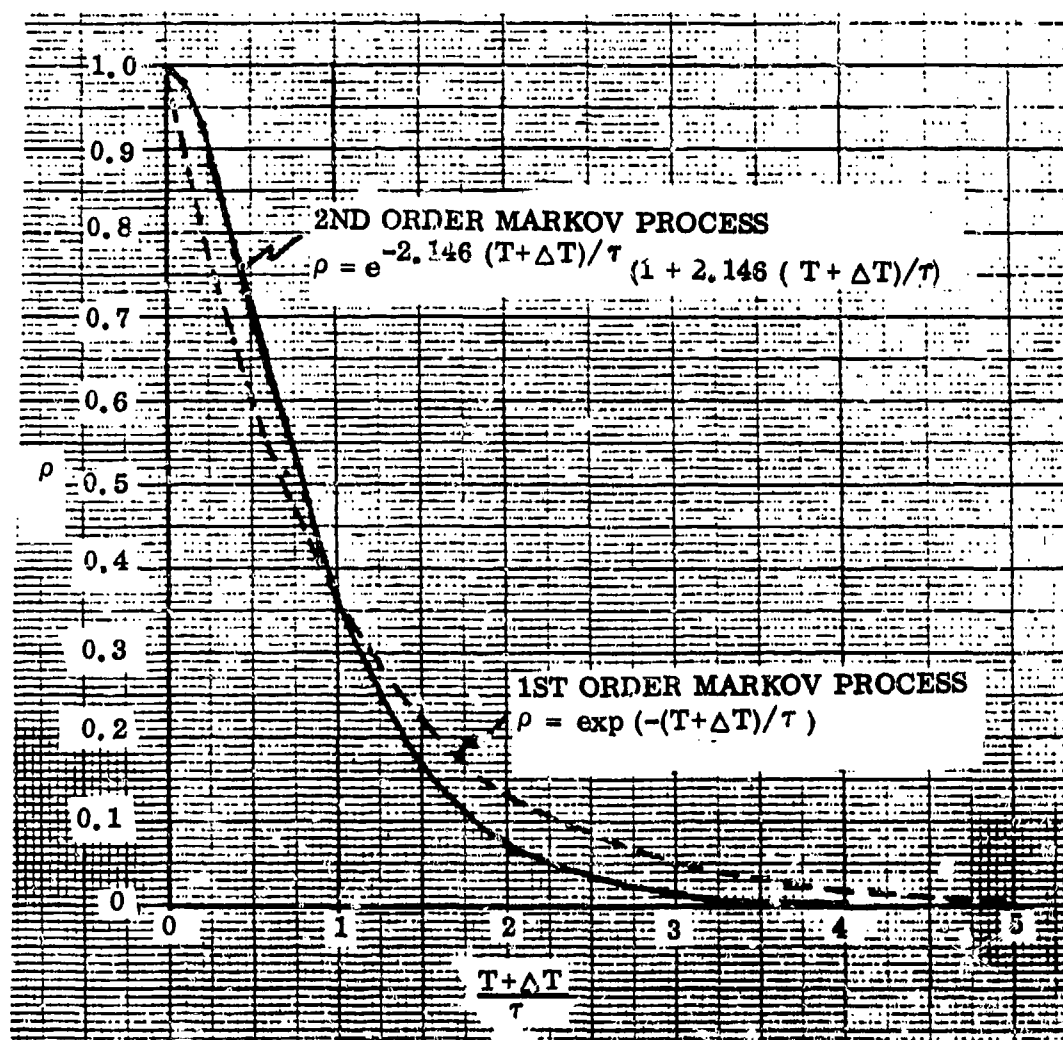


Figure 5-2. Correlation as a Function of the Ratio of Flight Cycle Time to Bias Correlation Period

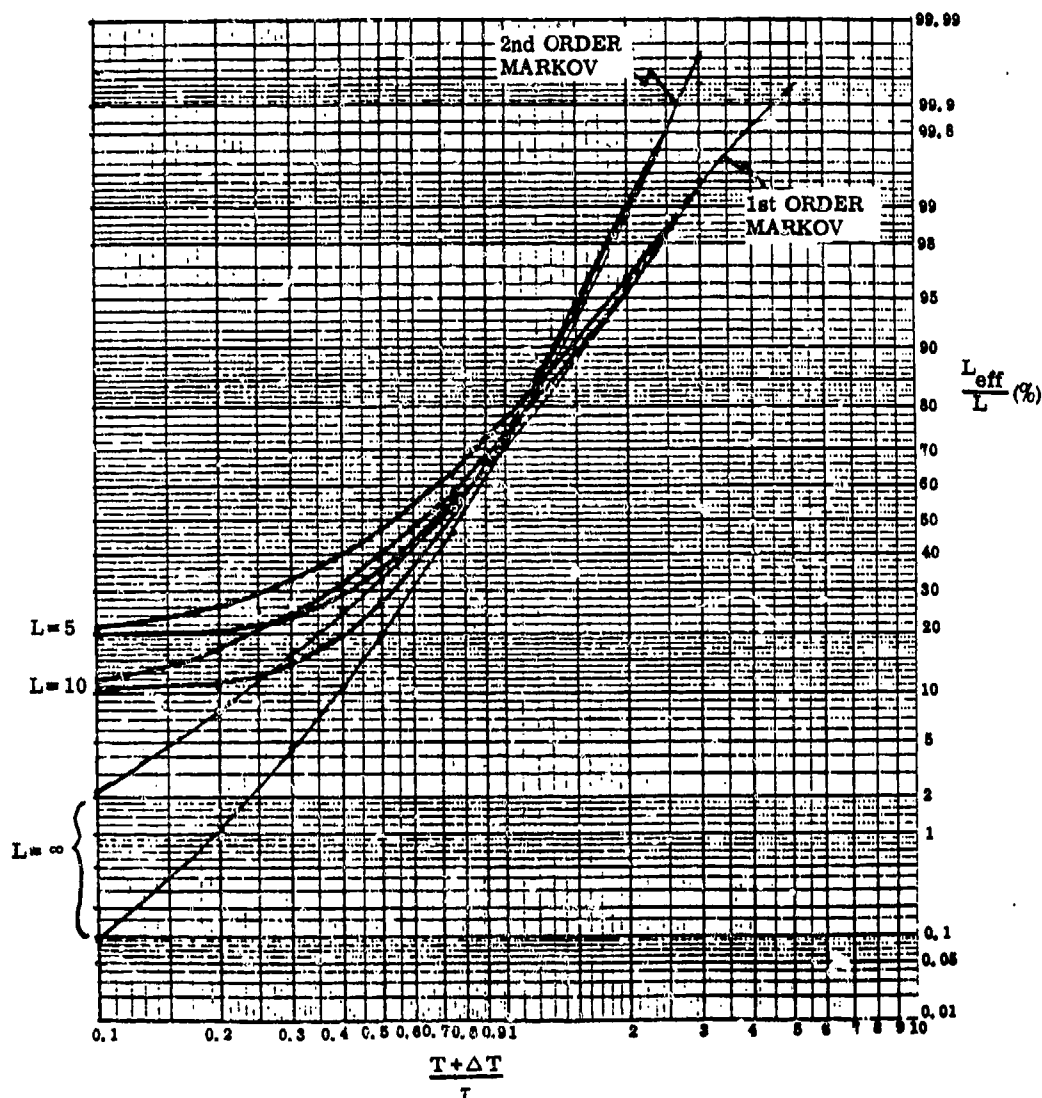


Figure 5-3. Effective Number of Independent Legs vs Ratio of Flight Cycle Time to Bias Correlation Period with Number of Legs as a Parameter

$$K = \begin{cases} 3.85 \text{ mrad}; & R \leq R_o \\ 0.53 \text{ mrad}; & R > R_o \end{cases} \quad (5-16)$$

and a waveform change at $R_o = 80 \text{ nmi}$, for example.

Typical equipment bias errors are

$$\sigma_e = \begin{cases} 0.6 \text{ mrad}; & R \leq R_o \\ 0.5 \text{ mrad}; & R > R_o \end{cases} \quad (5-17)$$

The rms residual refraction error after correction using the National Bureau of Standards (NBS) standard is given in Figures 3(a) and (b) of reference 4. An analytical fit in the region of interest to us is as follows:

$$\sigma_A = \frac{12}{|E|^{0.6183} e^{0.2 (\ln |E|)^2}} \quad (5-18)$$

The error variance σ_{ALT}^2 is identified as the Mode-C height error variance without radiosonde correction and in the absence of atmospheric pressure variability. The sources of uncertainty are altimeter pressure measurement error and encoding error. As such, it is independent from point-to-point. From Equation (3-6),

$$\sigma_{ALT}^2 = \frac{\left(\frac{b}{2a}\right)^2}{(1 + H/a)^2} \left(\frac{\sigma_{p_m}}{p}\right)^2 + \sigma_{H_{enc}}^2 \quad (5-19)$$

where

$$\sigma_{H_{enc}} = 0.065 \text{ kft} \quad (5-20)$$

and

$$\sigma_{p_m} = 3 \text{ mb.} \quad (5-21)$$

The error variance σ_{VAR}^2 is identified as the Mode-C height error variance without radiosonde correction and in the absence of altimeter error. The sources of uncertainty are the temporal and spatial variability of pressure at the surface and at altitude. It seems reasonable to assume that this error source is independent only from leg-to-leg. Again from Equation (3-6),

$$\begin{aligned} \sigma_{\text{VAR}}^2 = & \frac{\left(\frac{b}{2a}\right)^2}{(1+H/a)^2} \left(\frac{\sigma_{p_\infty}}{p}\right)^2 + \left[\frac{1}{c} + \frac{2(p_{\text{SL}}-p_o)}{d}\right]^2 \sigma_{p_{\text{SL}}}^2 \\ & - \frac{b}{a} \left[\frac{1}{c} + \frac{2(p_{\text{SL}}-p_o)}{d}\right] \frac{\sigma_{p_{\text{SL}}}}{(1+H/a)} \left(\frac{\sigma_{p_\infty}}{p}\right) e^{\frac{-H}{4.63}} \left[1 + \frac{H}{4.63}\right] \end{aligned} \quad (5-22)$$

where,

$$\sigma_{p_{\text{SL}}} = 0.032 p_o, \quad (5-23)$$

and

$$\begin{aligned} a &= 204.8 \text{ kft}, \\ b &= (103.33 \text{ kft})^2, \\ c &= 36.922 \text{ mb/kft}, \\ d &= (269.503)^2 \text{ mb}^2/\text{kft}, \text{ and} \\ p_o &= 1013.25 \text{ mb}. \end{aligned}$$

The error variance σ_{RAD}^2 is the variance of the Mode-C height error after radiosonde correction in the absence of altimeter error. Thus from Equation (4-1),

$$\sigma_{\text{RAD}}^2 = \left(\frac{\hat{H}_{nl}^c}{\ln \frac{p_{i+1}}{p_i}} \right)^2 \left[\left(1 - \frac{H_{i+1}}{\hat{H}_{nl}^c} \right)^2 + \left(1 - \frac{H_i}{\hat{H}_{nl}^c} \right)^2 \left(\frac{p_i}{p_{i+1}} \right)^2 \right] \left(\frac{\sigma_p}{p_i} \right)^2 \quad (5-24)$$

where σ_p^2 is the variance of the smoothed radiosonde pressure at a given hydrostatic altitude as given in Figure 4-4. Note that this error is independent only from leg-to-leg.

The error variance σ_p^2 is the variance of the Mode-C height error after radiosonde correction in the absence of radiosonde error. This error is independent from data point to data point and also comes from Equation (4-1) as,

$$\sigma_{\text{RA}}^2 = \left(\frac{H_i - H_{i+1}}{\ln \frac{p_{i+1}}{p_i}} \right)^2 \left[\sigma_{H_{\text{enc}}}^2 \left(\frac{\ln \frac{p_{k+1}}{p_k}}{h_{k+1} - h_k} \right)^2 + \left(\frac{\sigma_{p_m}}{\hat{p}_{n,l}} \right)^2 \right] \quad (5-25)$$

The parameters which materially affect the uncertainty of the fixed height bias estimate are:

1. The ratio of the leg cycle time to the leg-to-leg correlation time, i.e., $(T + \Delta T)/\tau$.
2. The number of flight legs, L .
3. The flight altitude, H .

In order to expose these sensitivities, constant altitude radial flight legs were simulated with a target speed of about 500 knots and a data interval of 12 seconds. This gives about 7 data points per bias estimate, per leg. In Figure 5-4, ten legs were assumed with the aircraft at 40 kft. Three ratios of $(T + \Delta T)/\tau$ were selected, i.e. 0.1, 0.5, and 1.5 and the second-order Markov model was used for correlation. As it happens a ratio of 1.5 is almost equivalent to an infinite number of correlation-times between legs, or a leg-to-leg correlation of zero. Note the dramatic effect of radiosonde correction for all ranges below about 120 nmi. These curves say that if one is only concerned about fixed height biases of a few thousand feet, then it probably isn't necessary to use radiosonde

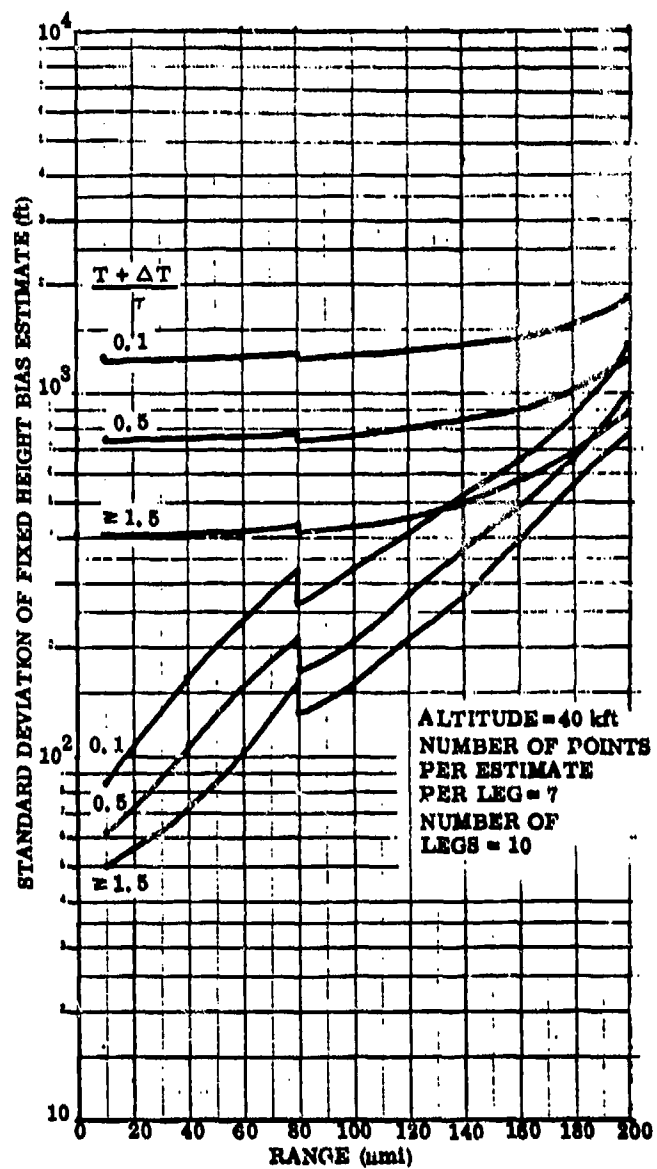


Figure 5-4. Standard Deviation of Fixed Height Bias Estimate
with and without Radiosonde Correction
- Effect of Correlation from Leg to Leg

so long as $T + \Delta T \geq 1.5 \tau$. On the otherhand, if fixed height biases of a few hundred feet can be worrisome then radiosonde correction is essential.

The effect of the number of legs is shown in Figure 5-5 with $T + \Delta T \geq 1.5 \tau$, $N=7$, and $H=40$ kft. Here we can see the value in using 10 legs but probably not for 30, particularly with radiosonde correction. (This question may require revisiting when we consider the statistical risk).

Finally consider the effect of aircraft altitude. Results for altitudes of 10, 20, 30, and 40 kft are plotted in Figure 5-8 where $N=7$, $H=10$, and $(T + \Delta T) \geq 1.5 \tau$. The strange resonance-like behavior at 10 and 20 kft derive from the fact that at these peaks the elevation angle is zero and the uncertainty from atmospheric refraction is dominant. This effect is so dominant that radiosonde correction is totally useless. Of course for a sea level site the far side of these peaks cannot be seen by the radar as they correspond to negative elevation angles. Nevertheless these curves do provide at least qualitative effects for raised sites where negative angles are possible.

5.4 STATISTICAL RISKS

Since the error distribution of $\hat{c} - c$ is zero-mean Gaussian with variance $\sigma_{\hat{c}}^2$ (Equation (5-13)), pass/fail thresholds are easily formulated in terms of risks. The producer's maximum risk is the probability of failing the test, i. e. $|\hat{c}| > |C_{P/F}|$ where $|C_{P/F}|$ is the pass/fail threshold, given that the true fixed bias error (in the absence of sampling uncertainty) is zero, i. e. false failure. Thus,

$$R_{\hat{c}}^P = P_r \left[|\hat{c}| > |C_{P/F}| / |c| = 0 \right] . \quad (5-26)$$

The buyer's maximum risk is the probability of passing the test, i. e. $|\hat{c}| \leq |C_{P/F}|$, given that the true fixed bias error $|c|$ is his maximum tolerated fixed bias error $|C_B|$, i. e., false passing. Thus,

$$R_{\hat{c}}^B = P_r \left[|\hat{c}| \leq |C_{P/F}| / |c| = |C_B| \right] \quad (5-27)$$

These risks are illustrated in Figure 5-7. Evaluated in terms of error functions,

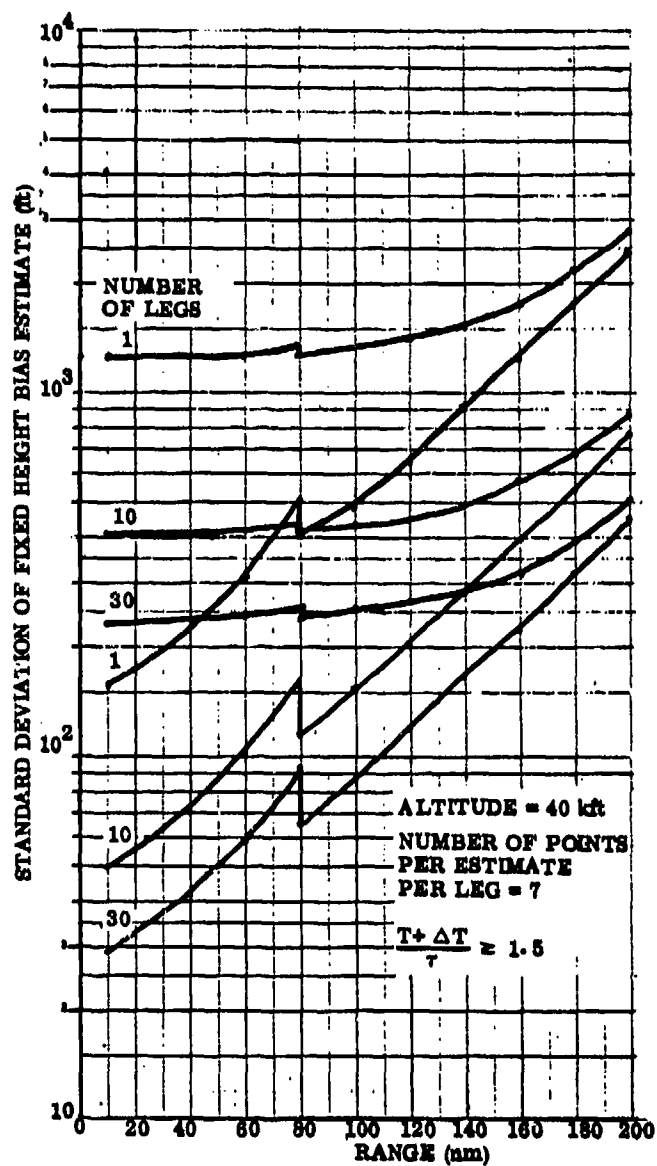


Figure 5-5. Standard Deviation of Fixed Height Bias Estimate
with and without Radiosonde Correction
- Effect of Number of Legs

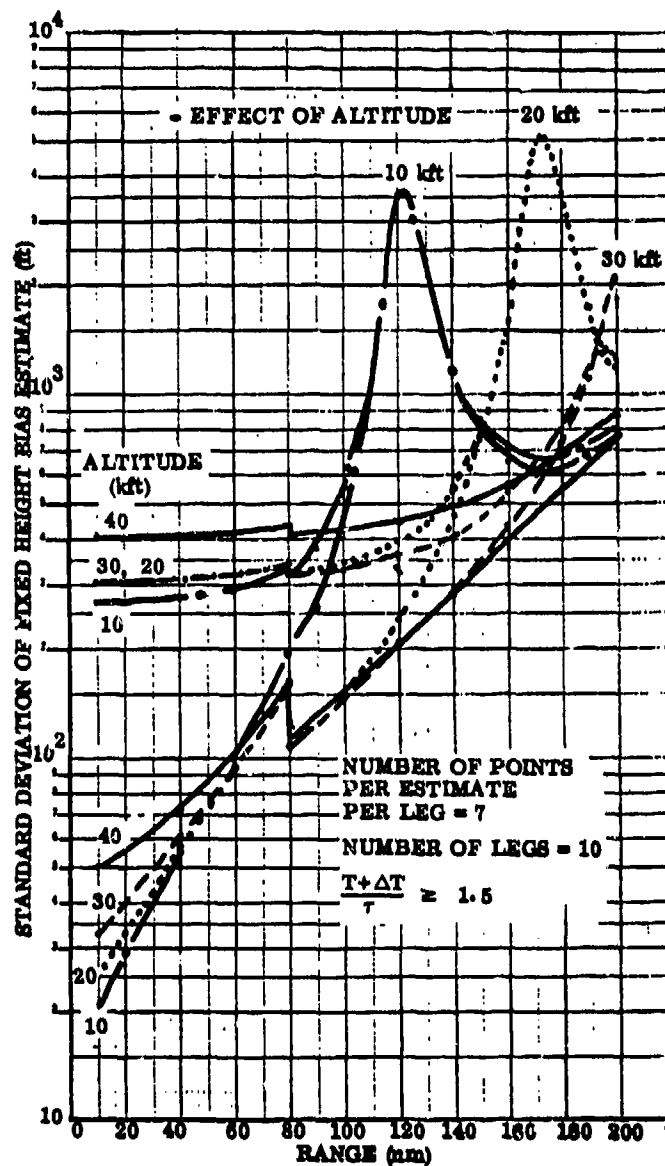


Figure 5-6. Standard Deviation of Fixed Height Bias Estimate
with and without Radiosonde Correction
- Effect of Altitude

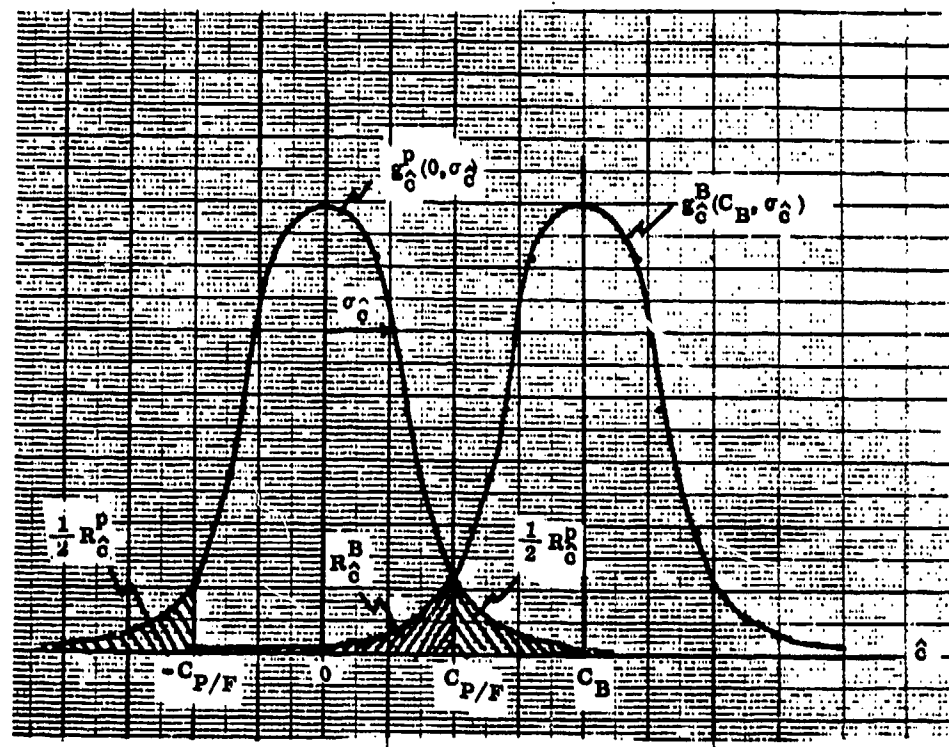


Figure 5-7. Schematic Distributions of Estimation Error for Producer and Buyer Showing Risks as Shaded Areas

$$\begin{aligned}
R_{\hat{C}}^P &= 1 - \int_{-|C_{P/F}|}^{|C_{P/F}|} \frac{1}{\sqrt{2\pi}\sigma_{\hat{C}}} \exp \left\{ -\frac{1}{2} \left(\frac{x}{\sigma_{\hat{C}}} \right)^2 \right\} dx \\
&= 1 - \operatorname{erf} \left(\frac{|C_{P/F}|}{\sqrt{2}\sigma_{\hat{C}}} \right), \tag{5-28}
\end{aligned}$$

and

$$\begin{aligned}
R_{\hat{C}}^B &= \int_{-|C_{P/F}|}^{|C_{P/F}|} \frac{1}{\sqrt{2\pi}\sigma_{\hat{C}}} \exp \left\{ -\frac{1}{2} \left(\frac{x - |C_B|}{\sigma_{\hat{C}}} \right)^2 \right\} dx \\
&= \frac{1}{2} \left[\operatorname{erf} \left(\frac{|C_{P/F}| - |C_B|}{\sqrt{2}\sigma_{\hat{C}}} \right) + \operatorname{erf} \left(\frac{|C_{P/F}| + |C_B|}{\sqrt{2}\sigma_{\hat{C}}} \right) \right] \tag{5-29}
\end{aligned}$$

with

$$\operatorname{erf}(x) \triangleq \frac{2}{\sqrt{\pi}} \int_0^x e^{-t^2} dt. \tag{5-30}$$

These risks are plotted in Figures 5-8 and 5-9, respectively, for typical ranges of the parameters $|C_{P/F}|/\sigma_{\hat{C}}$ and $|C_B|/\sigma_{\hat{C}}$. Note that once a producer's risk is allocated from an overall risk level down to the marginal risk for the height bias test, that the pass/fail threshold only depends on the uncertainty of the estimate, i. e. as measured by $\sigma_{\hat{C}}$, the quantity evaluated in the previous section. The buyer's position is not symmetrical with the producer's position however in that his least acceptable performance (as represented by the buyer's limit $|C_B|$) depends on the pass/fail threshold as well as $\sigma_{\hat{C}}$, for a given allocated buyer's risk.

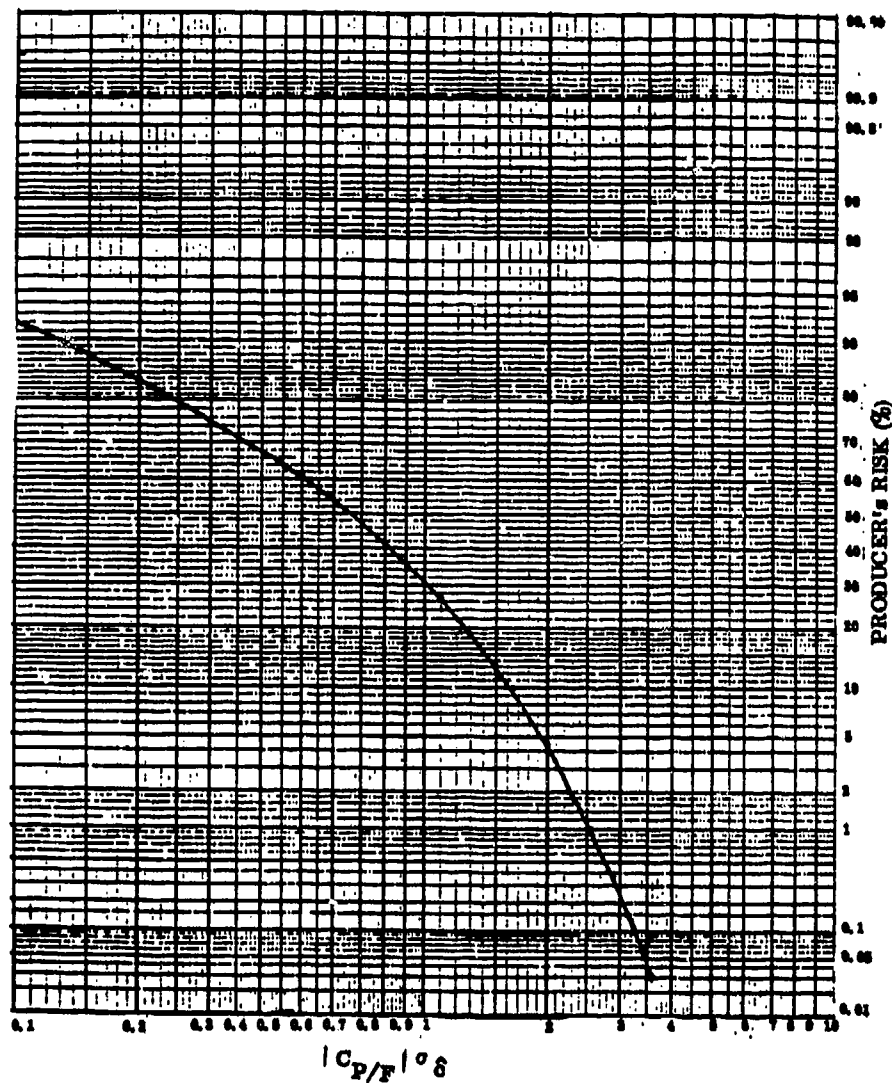


Figure 5-8. Producer's Risk vs Normalized Pass/Fail Threshold

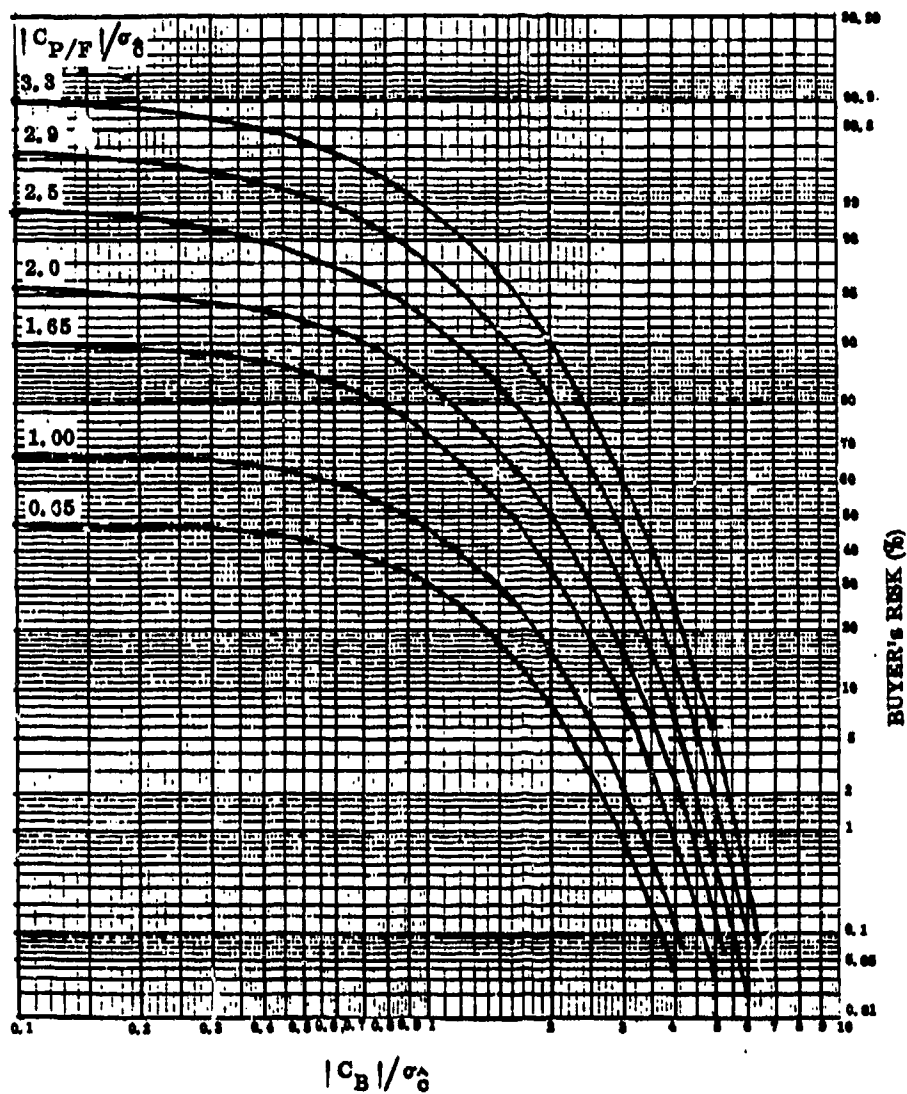


Figure 5-9. Buyer's Risk vs Normalized Maximum Tolerable Fixed Bias Error with Normalized Pass/Fail Threshold as a Parameter

Before fixing ideas further with numerical samples, it is helpful to understand the risk allocation process so that we can assess realistic risk levels.

5.5 OVERALL TEST STRUCTURE

Before we can go back to the application where we quantified typical values for the uncertainty in the bias estimate and to apply these values to help gauge pass/fail thresholds, we must first assess the levels of reasonable risk. A mutually acceptable range of overall acceptance test risks appears to be between 5 and 10%. That is, the risk of the producer falsely failing or falsely passing the controlled-flight acceptance test merely because of inadequate sample sizes is between 5 and 10%. The bias test is only one component of the overall test. In fact, as many as 14 independent performance measures can be tested, i. e. ,

1. Probability of detection
2. Absolute range accuracy
3. Absolute height accuracy
4. Absolute azimuth accuracy
5. 95th percentile absolute height accuracy
- 6, 7. Relative height accuracy between closely spaced and distantly spaced targets
- 8, 9. 95th percentile relative height accuracy between closely spaced and distantly spaced targets
- 10, 11. Range resolution between targets of equal and unequal radar cross section (RCS)
- 12, 13. Azimuth resolution between targets of equal or unequal radar cross section (RCS)
14. Height (or elevation) bias test

where absolute accuracy refers to a single aircraft and can include bias in an rms sense or just involve the variance. Relative accuracy implies two aircraft. There can be as many as four separate altitudes or types of environmental conditions tested and separate pass/fail thresholds established for as many as 20-range intervals per radial leg. Thus, there can be hundreds of separate pass/fail thresholds for an acceptance test with an overall risk between 5 and 10%.

5.5.1 PASS/FAIL CRITERIA

What must the allocated risk be on the level of a single range interval (where pass/fail thresholds are applied)? This depends upon the criterion for passing the overall test. If the producer must pass each and every subtest to pass the acceptance test, then the producer's risk will add up rapidly and his risk per subtest must be very small indeed. If the allocated risk per lowest level subtest r^P is equal for all subtests, then for an overall risk level of R^P ,

$$R^P = 1 - (1 - r^P)^{N_s} \quad (5-31)$$

where N_s is the number of subtests. Similarly for the buyer, there are so many ways for the producer to fail that the buyer's risk per lowest-level subtest will reduce rapidly. If the overall risks to buyer and producer are to be about equal (seems reasonable) then the buyer's subtest risk r^B must be fairly large. In fact

$$R^B = (r^B)^{N_s} \quad (5-32)$$

These equations are easily solved for r^P and r^B and are plotted in Figures 5-10 and 5-11 as the curve marked $M=0$, where M is the total number of subtest failures permitted for the producer to pass the acceptance test. Note that for 10 subtests the producer's risk per subtest must be as low as 1% to achieve an overall level of 10%. Moreover, for $N_s = 100$, $r^P \approx 0.1\%$. Similarly, for 10 subtests the buyer must endure a risk per subtest of almost 80%. And when $N_s = 100$, $r^B \approx 98\%$. Buyers often chafe at this notion (although perfectly true) and seek to relieve this pressure while simultaneously raising the producer's subtest risk by permitting the producer to fail a few subtests while still passing the acceptance test itself. Quantitatively,

$$R^P = \sum_{n=M+1}^{N_s} \frac{N_s!}{n! (N_s-n)!} (r^P)^n (1-r^P)^{N_s-n} \quad (5-33)$$

and

$$R^B = \sum_{n=N_s-M}^{N_s} \frac{N_s!}{n! (N_s-n)!} (r^B)^n (1-r^B)^{N_s-n} \quad (5-34)$$

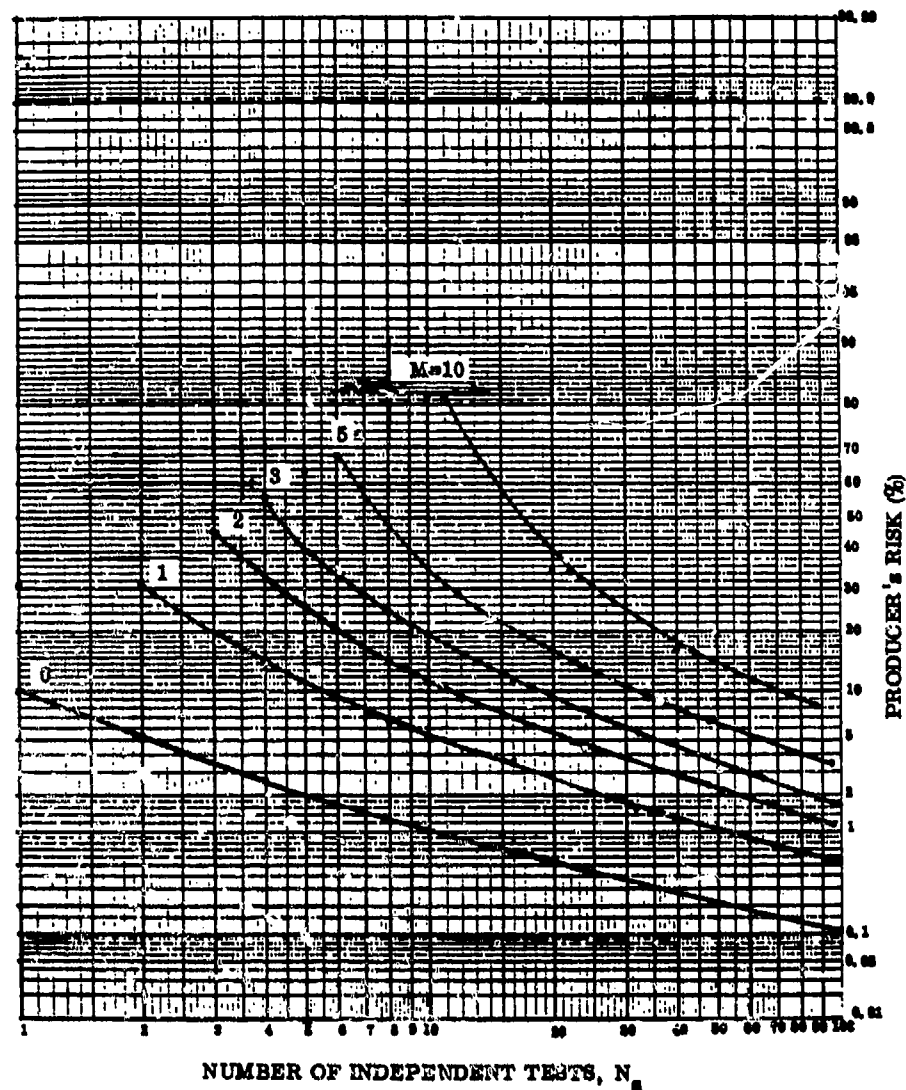


Figure 5-10. Producer's Risk per Test vs Total Number of Tests with Overall Risk of 10% and the Number of Permitted Failures as a Parameter

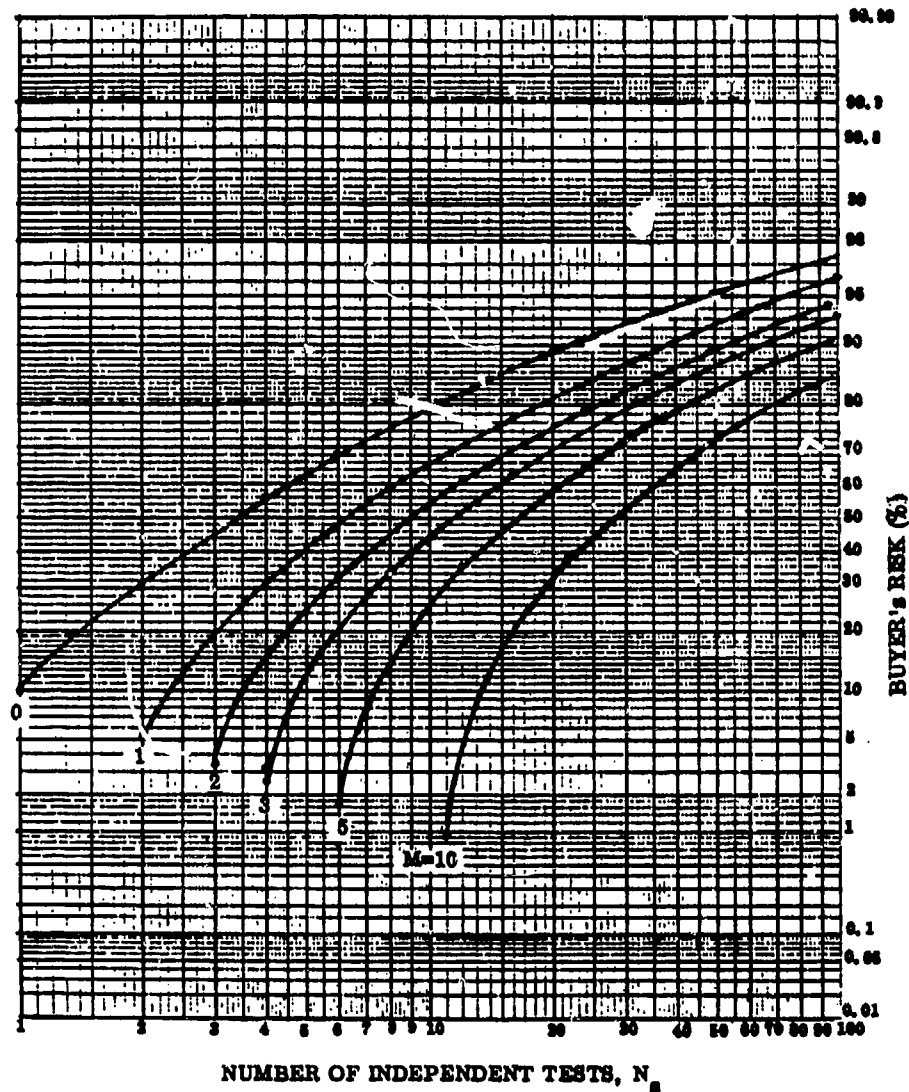


Figure 5-11. Buyer's Risk per Test vs Total Number of Tests with Overall Risk of 10% and the Number of Permitted Failures as a Parameter

The remaining curves in Figures 5-10 and 5-11 show the effects of permitting 1 to 10 total subtest failures. An interesting way to gauge the effectiveness of this procedure is to consider an exercise whereby the producer's risk per subtest remains at the overall level (say 10%). The first column of the following table shows the required number of tests for this to occur for M between 0 and 10. The third and fourth columns give the corresponding producer's and buyer's subtest risks. Compare these to the last two columns which must be obtained for no permitted failures. The contrast is marked. As we'll see shortly, the corresponding pass/fail thresholds and the buyer's maximum-tolerated fixed bias level will also be affected.

N	M	$r_M^P(\%)$	$r_M^B(\%)$	M	$r_O^P(\%)$	$r_O^B(\%)$
1	0	10	10	0	10	10
5	1	10	40	0	2	62
11	2	10	58	0	0.9	81
18	3	10	66	0	0.6	88
32	5	10	77	0	0.35	93.8
70	10	10	80	0	0.15	96.5

5.5.2 PASS/FAIL THRESHOLDS

Now we can combine the estimation uncertainty σ_0 and pass/fail criteria into pass/fail thresholds and buyer's limits. Figure 5-12 is a plot of the pass/fail threshold versus range. Here we have selected the case where the flight cycle time is long enough with respect to the bias error correlation period, i.e., $T + \Delta T \geq 1.5 \tau$, that the legs are effectively independent. Moreover we consider the case for 10 legs with and without correction to the Mode-C height and three levels of produce's subtest risk, i.e., 0.1%, 1%, and 10%. From Figure 5-12 we can see a dramatic difference at close ranges with and without radio-sonde correction. For example, at 60nmi and $r^P = 0.1\%$, $|C_{P/F}| = 1400$ ft without correction and only 340 ft with compensation, almost a factor of 4. At 200 nmi, however,

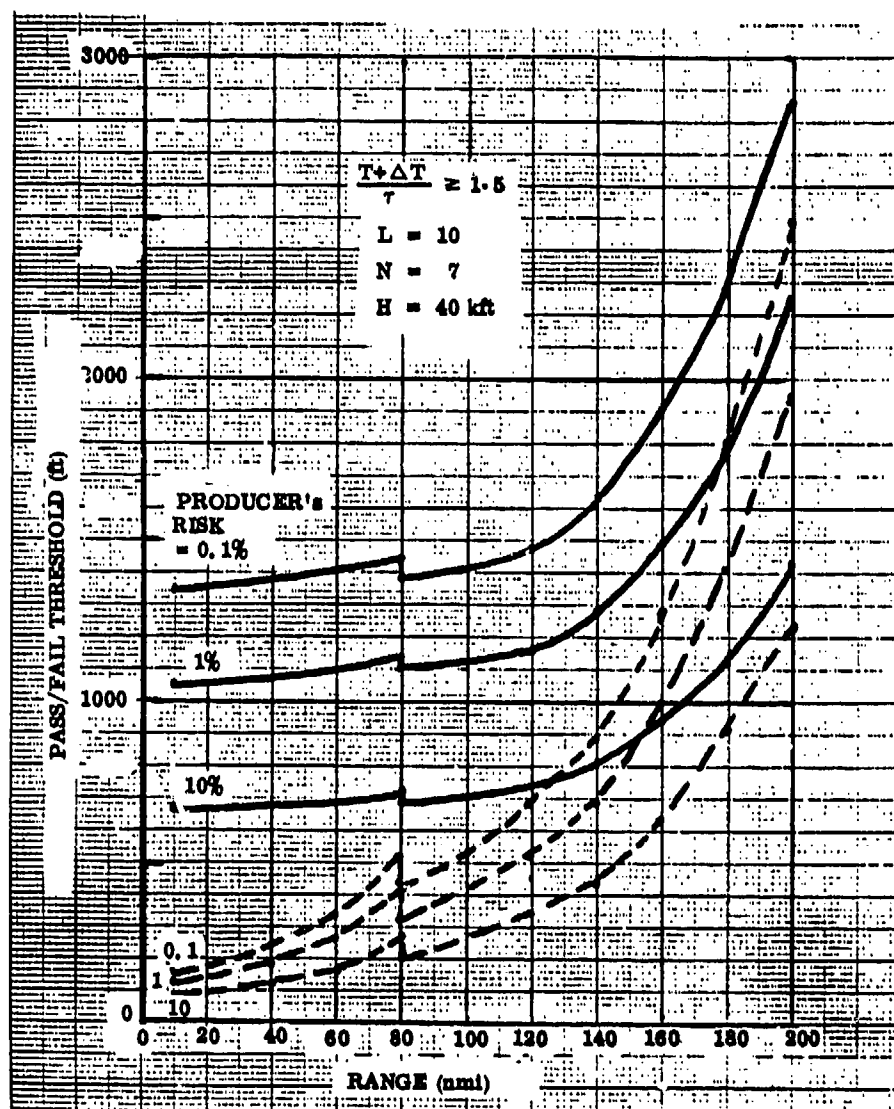


Figure 5-12. Pass/Fail Threshold vs Range for Fixed Height Bias Error at Producer's Risks of 0.1, 1, and 10%

the estimation error is dominated by thermal errors which cannot be adequately reduced even with 7 data points per range interval and 10 legs (intervals per subtest) for a total of 70 samples. Thus, for $r^P = 0.1\%$ $|C_{P/F}| = 2850$ ft without compensation and still as high as 2500 ft even after altimeter correction. The value of radiosonde corrections is then questionable for ranges beyond about 120 nmi.

The question of the maximum fixed bias the buyer must tolerate to accommodate sampling uncertainty is addressed next. Consider two contrasting criteria for passing:

1. $M=0$ (no permitted failures)

For $R^P=R^B = 10\%$, from Figures 5-10 and 5-11

$$r_0^P = 0.15\%; r_0^B = 96.5\%.$$

From Figures 5-8 and 5-9,

$$|C_{P/F}| = 3.20 \sigma_{\hat{C}}; |C_B|_0 = 1.4 \sigma_{\hat{C}}.$$

2. $M=10$ (10 out of 70 permitted failures)

For $R^P=R^B = 10\%$, from Figures 5-10 and 5-11

$$r_{10}^P = 10\%; r_{10}^B = 80\%.$$

From Figures 5-8 and 5-9,

$$|C_{P/F}| = 1.6 \sigma_{\hat{C}}; |C_B|_{10} = 0.7 \sigma_{\hat{C}}.$$

Here we see an interesting phenomenon. The strategy of permitting some subtest failures does four good things for the buyer. First, it forces the producer's subtest risk up from 0.15% to 10%. Second, this forces the pass/fail threshold down from $3.2 \sigma_{\hat{C}}$ to $1.6 \sigma_{\hat{C}}$, a factor of 2. Third, the buyer's subtest risk reduces from 96.5% down to 80%. Finally, the buyer's limit reduces from $1.4 \sigma_{\hat{C}}$ for no permitted failures to $0.7 \sigma_{\hat{C}}$ for 10 out of 70 permitted failures, also a factor of 2. The buyer will usually have free choice here, tailoring his strategy to his particular interests and concerns. From the producer's standpoint, his total risk is being guaranteed in any case and he should be satisfied to give the buyer this degree of freedom. Figures 5-13 and 5-14 are plots of $|C_{P/F}|$ and $|C_B|$, respectively, for the two alternative strategies highlighted here. Once again, a striking conclusion is the limited benefit of compensating the Mode-C height beyond about 120 nmi and the tremendous desirability for doing it at closer ranges.

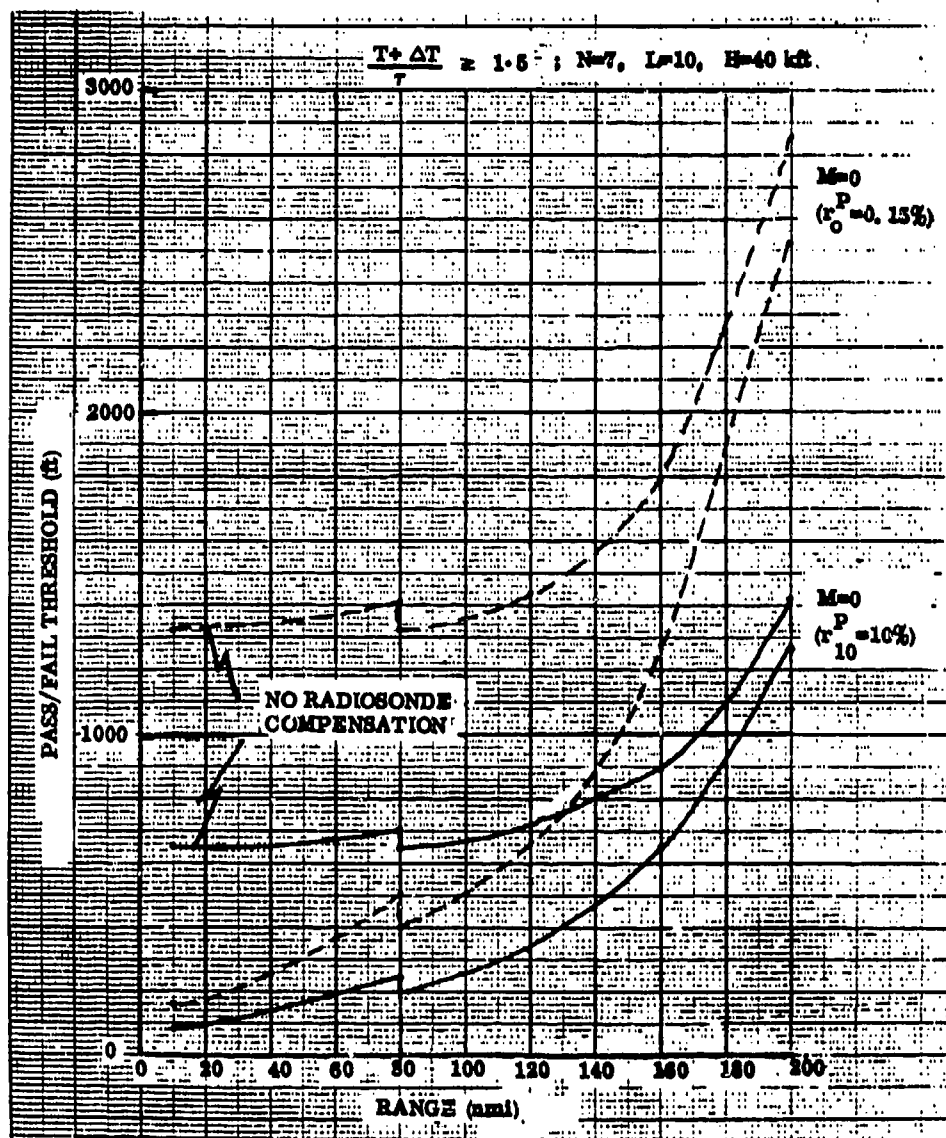


Figure 5-13. Pass/Fail Thresholds vs Range for 70 Subtests with Zero and 10 Permitted Subtest Failures and an Overall Risk of 10%

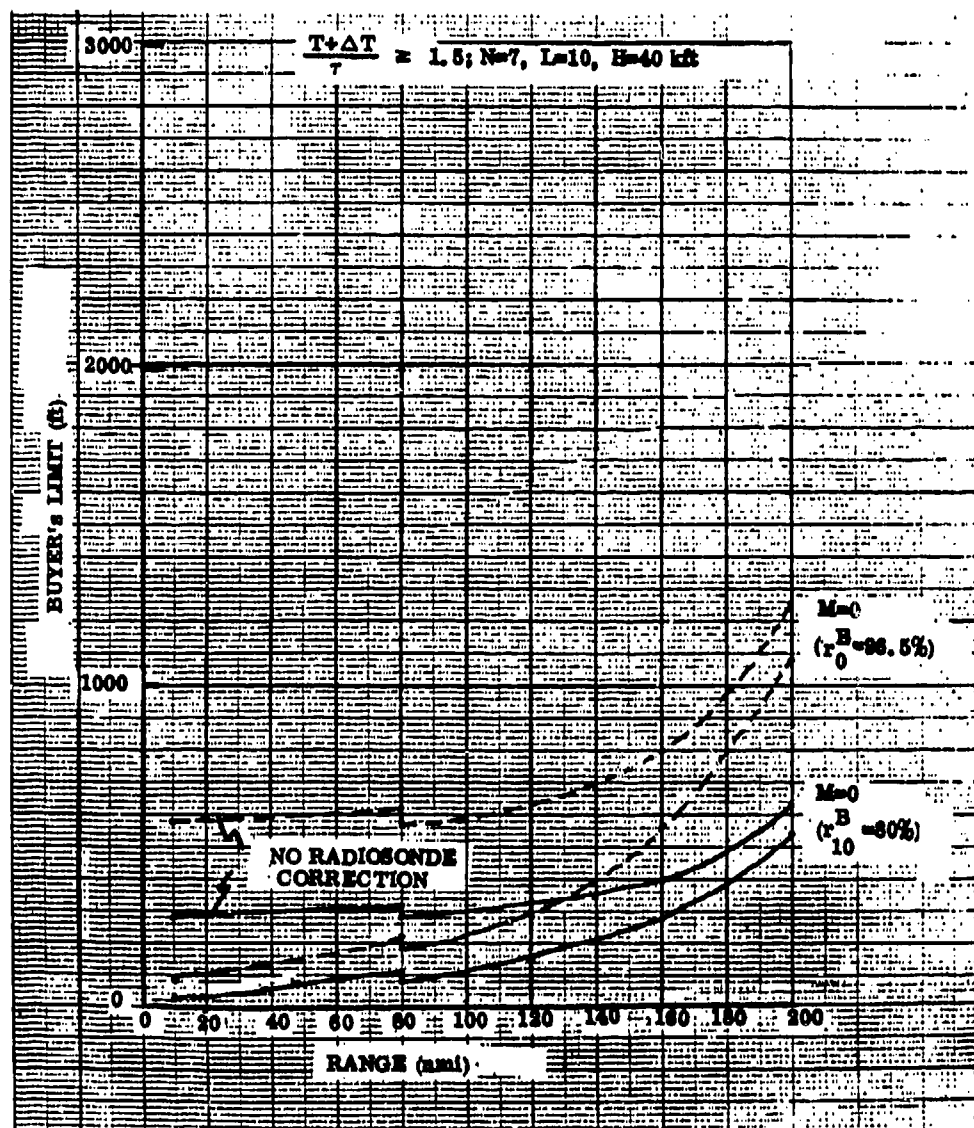


Figure 5-14. Maximum Tolerable Buyer's Limit of Fixed Height Bias vs Range for 70 Subtests with Zero and 10 Permitted Failures and an Overall Risk of 10%

5.5.3 TEST CONDUCT

Sometimes only one radiosonde will be available in the vicinity of a useful radial flight path and at appropriate times. Experience has shown that reasonable corrections to the altimeter can be made for ± 15 nmi about the radar range to the balloon. Figure 5-15 is a Range-Height-Angle chart which assumes that the radiosonde balloon ascended in the 70 to 80 nmi range window. Loosely interpreting this to a window of applicable altimeter corrections of from 60 to 90 nmi, we can see that four flight altitudes can cover all beams from 0.5° to 7° in elevation. Moreover, if a waveform change occurs at 80 nmi, these tests (at altitudes of 10, 18, 30, and 47 kft) will also test the height bias in both short-range and long-range beams.

Because we require no more than two bias flights a day (10-12 hours apart) at a given altitude, a sensible approach is to intersperse the bias flights with all other flights. For instance, at the end of each day before returning to base, the pilot can fly a single leg at each of the four altitudes (spiraling up or down between legs) in about the same time it takes to fly one leg from 0 to 200 nmi. Separate statistics are accumulated from day-to-day and separate thresholds applied at each of the four altitudes (in each 10 nmi range interval or in one 30 nmi interval) at the end of the allotted number of legs for the bias test.

5.6 ERROR ANALYSIS FOR THE MEAN-SQUARE HEIGHT ERROR TEST

In par. 5.3 through 5.5, we analyzed a test for uncovering a fixed bias error, the kind which results from an error in calibration, algorithmic compensation, or software. The buyer is primarily interested in this kind of error and already accepts the budgeted equipment bias error, which is random from day-to-day, i. e., $N(0, \sigma_\epsilon)$. He is protected from larger than promised values of σ_ϵ because the pass/fail thresholds are calculated from that value. The second test type accomplishes similar goals, but involves a threshold on the total mean square height error in the 30 nmi window of applicable radiosonde corrections. In both cases, the variance of absolute height accuracy is estimated and thresholded separately in the remaining range intervals. In this section we develop the statistics of the total mean square error for this second test type and compute risks and pass/fail thresholds to exemplify and clarify the approach. Much of what we have already covered remains applicable.

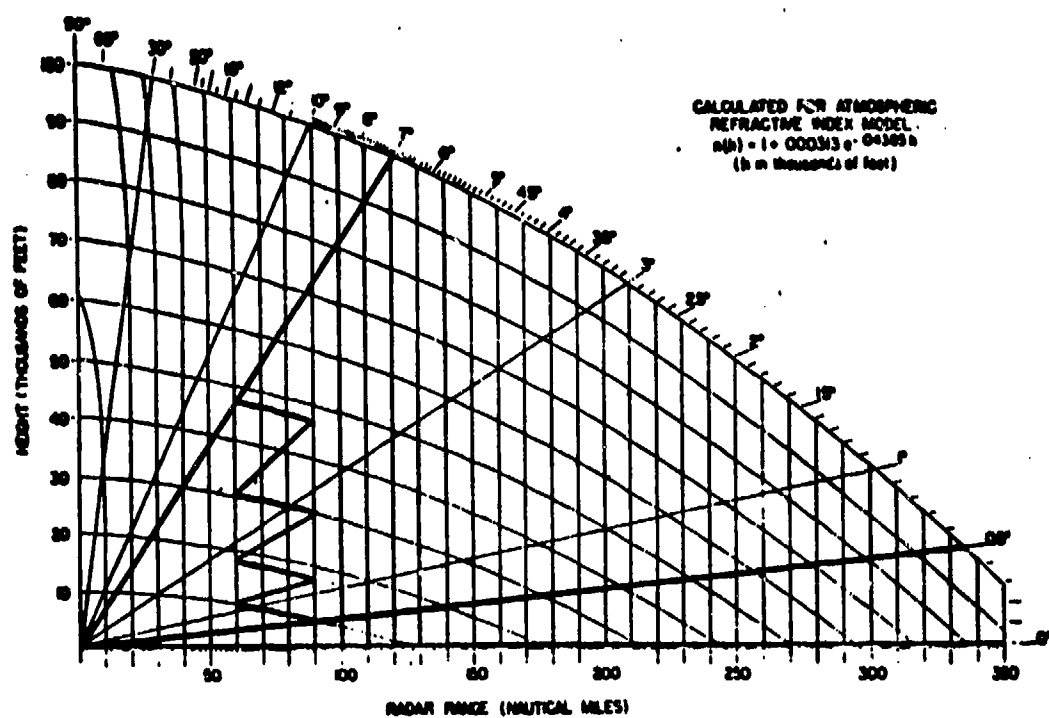


Figure 5-15. Typical Elevation Coverage for a Height Bias Test with a Radiosonde Ascent Between 70 and 80 nmi Range

5.6.1 DEFINITIONS

\hat{MSE}	total mean-square error estimate,
\tilde{H}_{ln}	the height residual for the n^{th} data point and l^{th} leg, i. e., $H^R - H^C$, where the altimeter has been corrected for temperature,
$\sigma_{\tilde{H}}$	standard deviation of the height residual,
λ, a, b, ν^*	parameters of the noncentral chi-square distribution,
χ	noncentral chi-square random variable,
χ_{ν}^2	standard chi-square random variable with ν degrees-of-freedom,
$f_x(x)$	probability density function of the random variable x at the value x , and
P_x	cumulative probability distribution of the random variable x .

5.6.2 VARIANCE OF THE ESTIMATE

The total mean-square error is the average squared difference between the primary and secondary height predictions with an adjustment for the residual root-mean-square (rms) refraction error, σ_A , if not included in the budget, and an altimeter presumed to be error-free (corrected for surface pressure and by radiosonde)*. Thus

$$\hat{MSE} \triangleq \frac{1}{LN} \sum_{l=1}^L \sum_{n=1}^L \left(H_{ln}^R - H_{ln}^C \right)^2 - \bar{R}^2 \sigma_A^2 \quad (5-35)$$

where,

$$\begin{aligned} H_{ln}^R - H_{ln}^C &\triangleq \tilde{H}_{ln} \\ &= C + \bar{R} \left(\alpha_{ln} + \beta_l \right) + \left(\delta H_{RA} \right)_{ln} + \left(\delta H_{RAD} \right)_l. \end{aligned} \quad (5-36)$$

* In this section we presume that $L_{\text{eff}} \approx L$ in that the test is conducted with flights no closer than 8-to 12-hours apart.

It is of interest to digress a moment to discuss the random error. It is easy to show that aircraft with mean flight paths that are cartesian linear, but not overflying the radar, can have equivalent polynomials in radar coordinate space that are quite high, especially at close range. Reliance upon simple flight path models, without a precision standard reference radar, can thus be shown to lead to inordinately large model errors that overwhelm the radar error. Here we are adequately correcting the altimeter in a few range intervals and any deviations from constant-height flight will show up identically in H^R and H^C . That is why we can estimate the total mean-squared error here with such confidence. In effect, we have created a precision reference standard.

Introducing Equation (5-36) into Equation (5-37) and noting that all the errors are $N(0, \sigma)$ and uncorrelated,

$$E(\hat{MSE}) = C^2 + \bar{R}^2 (\sigma_\sigma^2 + \sigma_\epsilon^2) + \sigma_{RA}^2 + \sigma_{RAD}^2 \quad (5-37)$$

which contains all the elements we wish to threshold, i.e., the point-to-point random error component σ_σ , the leg-to-leg random bias component σ_ϵ , the altimeter error after radio-sonde correction and any fixed bias term which may or may not be present. What is the error distribution of MSE? The distribution of the height residual \tilde{H}_{ln} is $N(C, \sigma_{\tilde{H}})$ where

$$\sigma_{\tilde{H}}^2 = \bar{R}^2 (\sigma_\sigma^2 + \sigma_\beta^2) + \sigma_{RA}^2 + \sigma_{RAD}^2 \quad (5-38)$$

Since

$$\hat{MSE} = \frac{1}{LN} \sum_l \sum_n \tilde{H}_{ln}^2 - \bar{R}^2 \sigma_A^2 \quad (5-39)$$

the distribution of $\sum_n \tilde{H}_{ln}^2 / \sigma_{\tilde{H}}^2$ is noncentral chi-square with N -degrees of freedom.

Thus,

$$\hat{MSE} = \frac{\sigma_{\tilde{H}}^2}{LN} \sum_l \chi_l^2(N, \lambda) - \bar{R}^2 \sigma_A^2 \quad (5-40)$$

where

$$\lambda \triangleq \sum_{n=1}^N \left(\mu_{\tilde{H}} \right)_n^2 / \sigma_{\tilde{H}}^2 = NC^2 / \sigma_{\tilde{H}}^2 . \quad (5-41)$$

The noncentral chi-square random variable which arises from the sum of the squares of non zero-mean Gaussian random variables with the same variance is a difficult distribution to work with. A common practice is to approximate it with a chi-square variable with appropriately adjusted moments (see reference 6, page 942). Thus

$$\chi^2(N, \lambda) \approx \chi_{\nu^*}^2(1+b), \quad (5-42)$$

where

$$b = \lambda / (N + \lambda), \quad (5-43)$$

$$a = N + \lambda, \quad (5-44)$$

and

$$\nu^* = \frac{a}{1+b} = \frac{(N + \lambda)^2}{N + 2\lambda} . \quad (5-45)$$

Note that,

$$f_{\chi_N^2}(t) = \frac{t^{\frac{N}{2} - 1} e^{-t/2}}{2^{N/2} \Gamma(N/2)} \quad (5-46)$$

with $\Gamma(x)$ the gamma function,

$$\Gamma(x) \triangleq \int_0^{\infty} t^{x-1} e^{-t} dt . \quad (5-47)$$

Now the sum of L chi-square random variables with ν^* degrees of freedom is still chi-square but with $L\nu^*$ degrees of freedom. Thus,

$$\hat{MSE} \approx \frac{(1+b) \sigma_{\tilde{H}}^2 \chi_{L\nu^*}^2}{LN} - \bar{R}^2 \sigma_A^2 . \quad (5-48)$$

Another way to look at this equation is to say that the random variable

$$\frac{LN}{(1+b) \sigma_H^2} \left(\hat{MSE} + \bar{R}^2 \sigma_A^2 \right) \cong \chi^2_{L\nu^*} \quad (5-49)$$

is approximately chi-square distributed with $L\nu^*$ degrees of freedom. What then is the distribution of \hat{MSE} ? Equation (5-48) is of the form

$$y = k_1 x - k_2$$

where x is chi-square. Then

$$f_Y(y) dy = f_X(x) dx$$

and

$$f_Y(y) = f_X \left(\frac{y+k_2}{k_1} \right) / k_1$$

or

$$f_{\hat{MSE}}(y) = \frac{LN \left[\frac{LN(y + \bar{R}^2 \sigma_A^2)}{(1+b) \sigma_H^2} \right]}{(1+b) \sigma_H^2} e^{-\frac{LN(y + \bar{R}^2 \sigma_A^2)}{(1+b) \sigma_H^2}} \cdot \frac{1}{2} \frac{L\nu^* - 1}{\Gamma(L\nu^*/2)} \quad (5-50)$$

Before making risk computations, it seems appropriate to check on the adequacy of the approximate formula for the noncentral chi-square distribution, i. e., Equations (5-42) through (5-45). A mathematical experiment was performed whereby the squares of ten samples from a Gaussian random number generator ($\sigma = 10$) were summed many times (i. e., 10000) and then histogrammed. In one case the Gaussian distribution was zero-mean, i. e., $N(0, 10)$, as a control. In the second case, the distribution was $N(10, 10)$. Here we are using $\nu = 10$, the lowest number of degrees-of-freedom of interest to us (about one-range interval worth). The empirical cumulative distributions are plotted in Figure 5-16 as triangles and circles for χ^2 and χ^2 respectively. The theoretical distributions are plotted

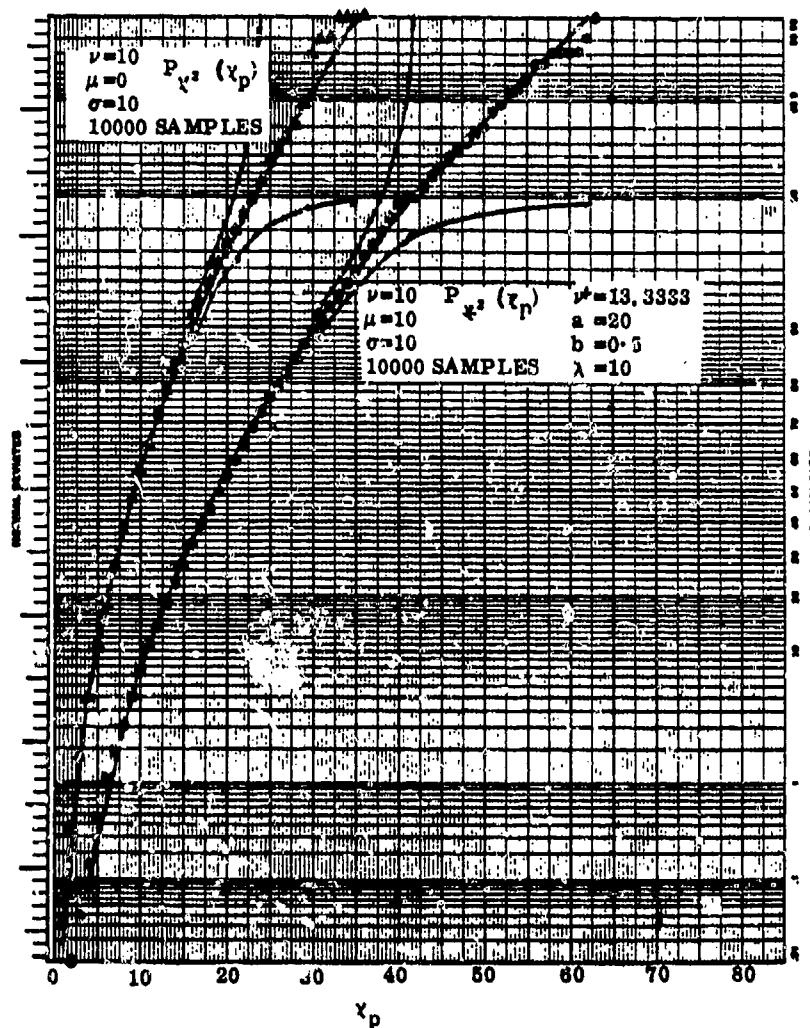


Figure 5-16. Theoretical and Experimental Probability Distributions for Chi-Square Central and Non-Central Random Variables

as the solid line running nearly perfectly through the data. In the χ^2 case, the approximation is used for the theoretical model. For the upper tail, I have also shown the 90% upper and lower confidence bounds for 10000 Monte-Carlos. Note how well the theoretical models fit the data from this point of view.

5.6.3 PRODUCER'S RISK

Unlike the distribution of $\hat{c} - c$, which was zero-mean Gaussian with variance $\sigma_{\hat{c}}^2$, the distribution of \hat{MSE} is much more complex, being related to the chi-square density function in Equation (5-50). But the formulation of risks is similar. The producer's risk of falsely failing due to inadequate sampling is

$$R_{\hat{MSE}}^P \triangleq P_r \left[\hat{MSE} > MSE_{P/F} / MSE \leq MSE_{P/F}; |c| = 0 \right] \quad (5-51)$$

where

- MSE is the true mean square error,
- \hat{MSE} is the sample estimate of MSE,
- $MSE_{P/F}$ is the pass/fail threshold, and
- $|c|$ is the magnitude of the fixed bias error.

Thus,

$$R_{\hat{MSE}}^P = \int_{MSE_{P/F}}^{\infty} f_{\hat{MSE}}^P(y) dy$$

where $f_{\hat{MSE}}^P(y)$ is given by Equation (5-50) with $|c| = 0$. Thus,

$$f_{\hat{MSE}}^P(y; |c| = 0) = \frac{LN}{\sigma_H^2} \frac{\left[\frac{LN(y + \bar{R}^2 \sigma_A^2)}{\sigma_H^2} \right] \exp \left\{ -\frac{1}{2} \left[\frac{LN(y + \bar{R}^2 \sigma_A^2)}{\sigma_H^2} \right] \right\}}{2^{LN/2} \Gamma(LN/2)} \quad (5-52)$$

Transforming variables, i.e.,

$$t \triangleq \frac{\text{LN} \left(y + \bar{R}^2 \sigma_A^2 \right)}{\sigma_{\tilde{H}}^2} \quad (5-53)$$

$$R_{\text{MSE}}^P = \int_{\frac{\text{LN} \left(\text{MSE}_{P/F} + \bar{R}^2 \sigma_A^2 \right)}{\sigma_{\tilde{H}}^2}}^{\infty} f_{\chi^2_{\text{LN}}} (t) dt \quad (5-54)$$

where $f_{\chi^2} (t)$ is just the chi-square distribution given in Equation (5-46).

5.6.4 PASS/FAIL THRESHOLDS

From Equation (5-54) we see a one-to-one relationship between $\text{MSE}_{P/F}$ and R^P with parameters LN , $\sigma_{\tilde{H}}^2$, and $\bar{R} \sigma_A$. The pass/fail threshold for $\sqrt{\text{MSE}_{P/F}}$ is plotted in Figure 5-17 for the same simulated test parameters as for the first test type, i.e., $L=10$, $N=7$, and the error budget previously described. The top two curves are shown for risks of 0.15% and 10% respectively. The bottom curve is a plot of $\sigma_{\tilde{H}}$ versus range showing how linear the pass/fail thresholds are in this parameter even with the complexity of Equation (5-54). It is important to reflect here that these computations imply radiosonde correction. Even though the root-MSE pass/fail threshold can be many thousands of feet for ranges beyond 120 nmi, it appears to be relatively insensitive to risk level.

5.6.5 BUYER'S RISK

Similarly to Equation (5-27),

$$R_{\text{MSE}}^B \triangleq P_r \left[\hat{\text{MSE}} \leq \text{MSE}_{P/F} / \text{MSE} > \text{MSE}_{P/F} ; |C| = |C_B| \right] \quad (5-55)$$

where $|C_B|$ is the maximum fixed bias error the buyer must tolerate due to sampling inadequacy. Thus,

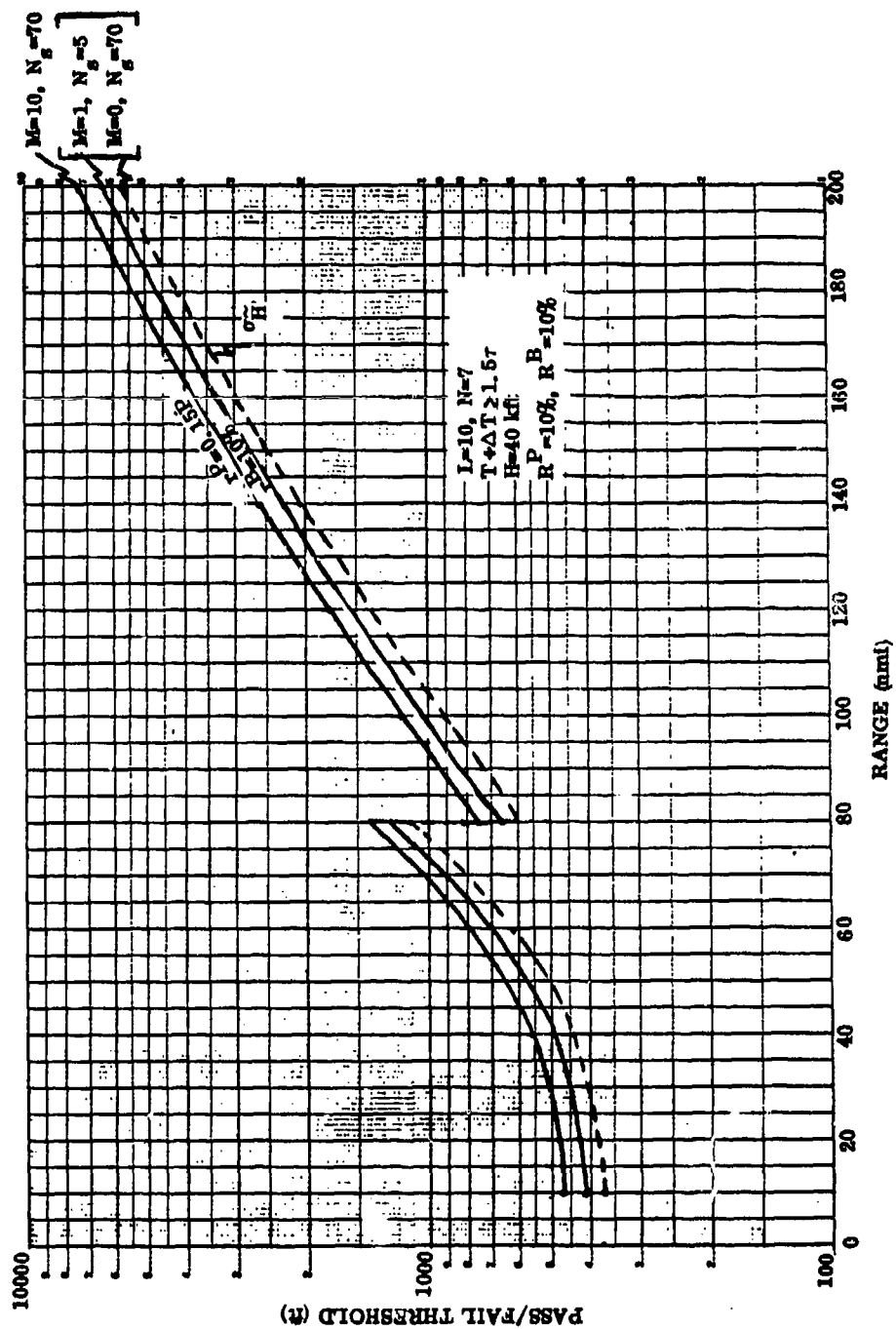


Figure 5-17. Pass/Fail Threshold for the Total Mean Square Height Error Test

$$R_{\hat{MSE}}^B = \int_{-\bar{R}^2 \sigma_A^2}^{MSE_{P/F}} f_{\hat{MSE}}(y, |C_B|) dy. \quad (5-56)$$

We will treat all negative estimates of \hat{MSE} (possible because of the correction factor $-\bar{R}^2 \sigma_A^2$) as zero. This is equivalent to considering only positive values of the distribution with an impulse at zero equivalent to the negative area. Thus,

$$R_{\hat{MSE}}^B = \int_0^{MSE_{P/F}} f_{\hat{MSE}}(y, |C_B|) dy + \int_{-\bar{R}^2 \sigma_A^2}^0 f_{\hat{MSE}}(y, |C_B|) dy \quad (5-57)$$

where the second term is the power of the impulse.

Making the variable transformation

$$t \triangleq \frac{LN}{(1+b) \sigma_{\tilde{H}}^2} (y + \bar{R}^2 \sigma_A^2) \quad (5-58)$$

we have,

$$R_{\hat{MSE}}^B = \frac{\frac{LN}{(1+b) \sigma_{\tilde{H}}^2} (MSE_{P/F} + \bar{R}^2 \sigma_A^2)}{LN \bar{R}^2 \sigma_A^2 / (1+b) \sigma_{\tilde{H}}^2} f_{\chi^2_{L\nu^*}}(t) dt + \int_0^{\frac{LN \bar{R}^2 \sigma_A^2}{(1+b) \sigma_{\tilde{H}}^2}} f_{\chi^2_{L\nu^*}}(t) dt, \quad (5-59)$$

with

$$\lambda = NC_B^2 / \sigma_{\tilde{H}}^2, \quad (5-60)$$

$$a = N + \lambda, \quad (5-61)$$

$$b = \lambda / (N + \lambda), \quad (5-62)$$

and

$$\nu^* = a/(1+b) = (N+\lambda)^2/(N+2\lambda). \quad (5-63)$$

Note that the second term has the same value whether we treat negative values of \hat{MSE} as zero or use them as they are. Thus we have that,

$$R_{MSE}^B = \int_0^{X_B} f_{\chi^2_{L\nu^*}}(t) dt \quad (5-64)$$

with

$$X_B \triangleq \frac{LN}{(1+b)\sigma_H^2} (y + \bar{R}^2 \sigma_A^2). \quad (5-65)$$

Solving Equations (5-59) thru (5-65) for X_B , b and $L\nu^*$ in terms of $|C_B|$, we get

$$X_B = \frac{LN(\sigma_H^2 + C_B^2)}{2C_B^2 + \sigma_H^2} \cdot \frac{(MSE_{P/F} + \bar{R}^2 \sigma_A^2)}{\sigma_H^2}. \quad (5-66)$$

$$L\nu^* = \frac{LN(\sigma_H^2 + C_B^2)^2}{(\sigma_H^2 + 2C_B^2)\sigma_H^2}, \quad (5-67)$$

and

$$b = C_B^2 / (\sigma_H^2 + C_B^2). \quad (5-68)$$

These equations provide a unique one-to-one relationship between $|C_B|$ and R_{MSE}^B with parameters LN , σ_H^2 , and $MSE_{P/F}$.

5.6.6 BUYER'S LIMIT FOR C_B

Equations (5-64) thru (5-67) are plotted in Figure 5-18 for a producer's risk of 10% and a buyer's risk of 10% overall. The topmost curve is the standard deviation of the height residual, $\sigma_{\tilde{H}}$. The other three curves are the buyer's limits on C for ($r^P = 10\%$, $r^B = 40\%$), ($r^P = 0.15\%$, $r^B = 96\%$), and ($r^P = 10\%$, $r^B = 80\%$) respectively corresponding to ($M=1$, $N_g=5$), ($M=0$, $N_g=70$), and ($M=10$, $N_g=70$) as before. Note that $|C_B|$ is larger in the MSE test than in the fixed height bias test. This is a consequence of summing over squared residuals instead of the residuals themselves as in the fixed height bias test. The comparison between the bottom two curves of Figure 5-18 is interesting. Here we see the material benefit to the buyer of permitting failures. At 120 nm' for instance the $M=0$ curve yields a buyer's limit of 620 feet. Permitting 10 out of 70 failures and allowing the producer to still pass the test reduces his limit on the fixed height bias of 380 feet, almost a factor of 2.

5.6.7 BUYER'S LIMIT ON MSE

From Equation (5-48) we have a general relationship between estimated MSE and the chi-square random variable. Thus,

$$\hat{MSE}_B = \frac{(1+b) \sigma_H^2 \chi_{L\nu}^2}{LN} - \bar{R}^2 \sigma_A^2. \quad (5-69)$$

The expected value of the mean-square buyer's limit corresponds to the expected value of the χ^2 -variable. Since

$$E \left(\chi_{L\nu}^2 \right) = L\nu, \quad (5-70)$$

$$E \left(\hat{MSE}_B \right) \triangleq MSE_B = (1+b) \sigma_H^2 \left(\frac{\nu^*}{N} \right) - \bar{R}^2 \sigma_A^2. \quad (5-71)$$

Introducing the expressions for b and ν^* in the terms of $|C_B|$ and then using the definition of $\sigma_{\tilde{H}}^2$, we find finally that

$$MSE_B = C_B^2 + \bar{R}^2 \left(\sigma_a^2 + \sigma_e^2 \right) + \sigma_{RA}^2 + \sigma_{RAD}^2. \quad (5-72)$$

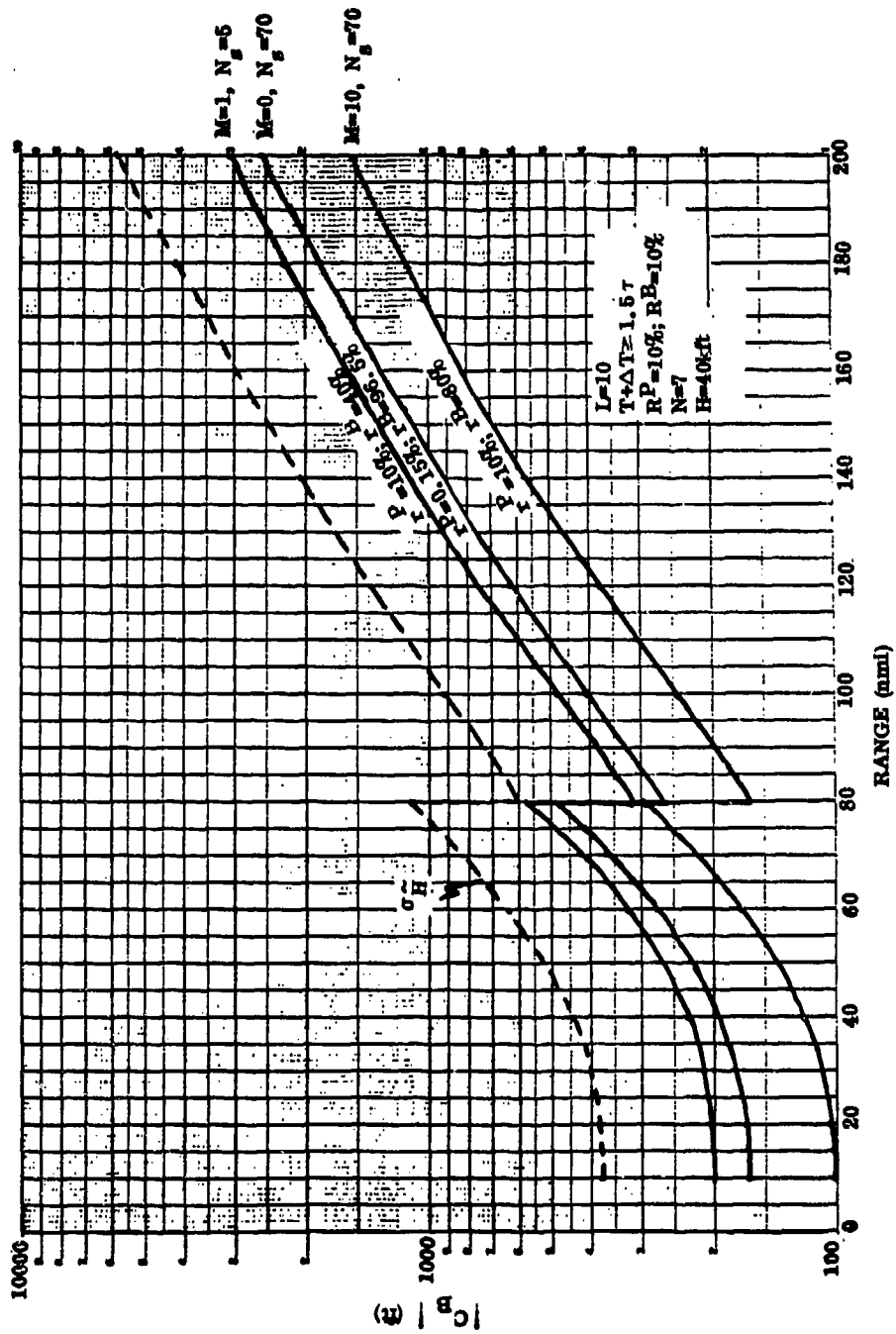


Figure 5-18. Maximum Tolerable Buyer's Limit on Fixed Height Bias Error as Part of a Total Mean Square Height Error Test

This is plotted in Figure 5-19 for the same pass/fail criteria of Figure 5-18. Once again, the curve for $\sigma_{\tilde{H}}$ is plotted (as a dashed line here) for comparison. Again, radiosonde data is presumed available to correct the Mode-C height. In this instance, unlike for the buyer's limit on the fixed component, i. e., $|C_B|$, there is only marginal benefit of permitting failures insofar as the buyer's limit on MSE is concerned. Nevertheless the buyer gains overall by forcing the producer's risk per subtest up from 0.15% to 10% and by reducing his risk per subtest down from 96.5% to 80%. His limit on the fixed component of height bias error is of course materially reduced as well.

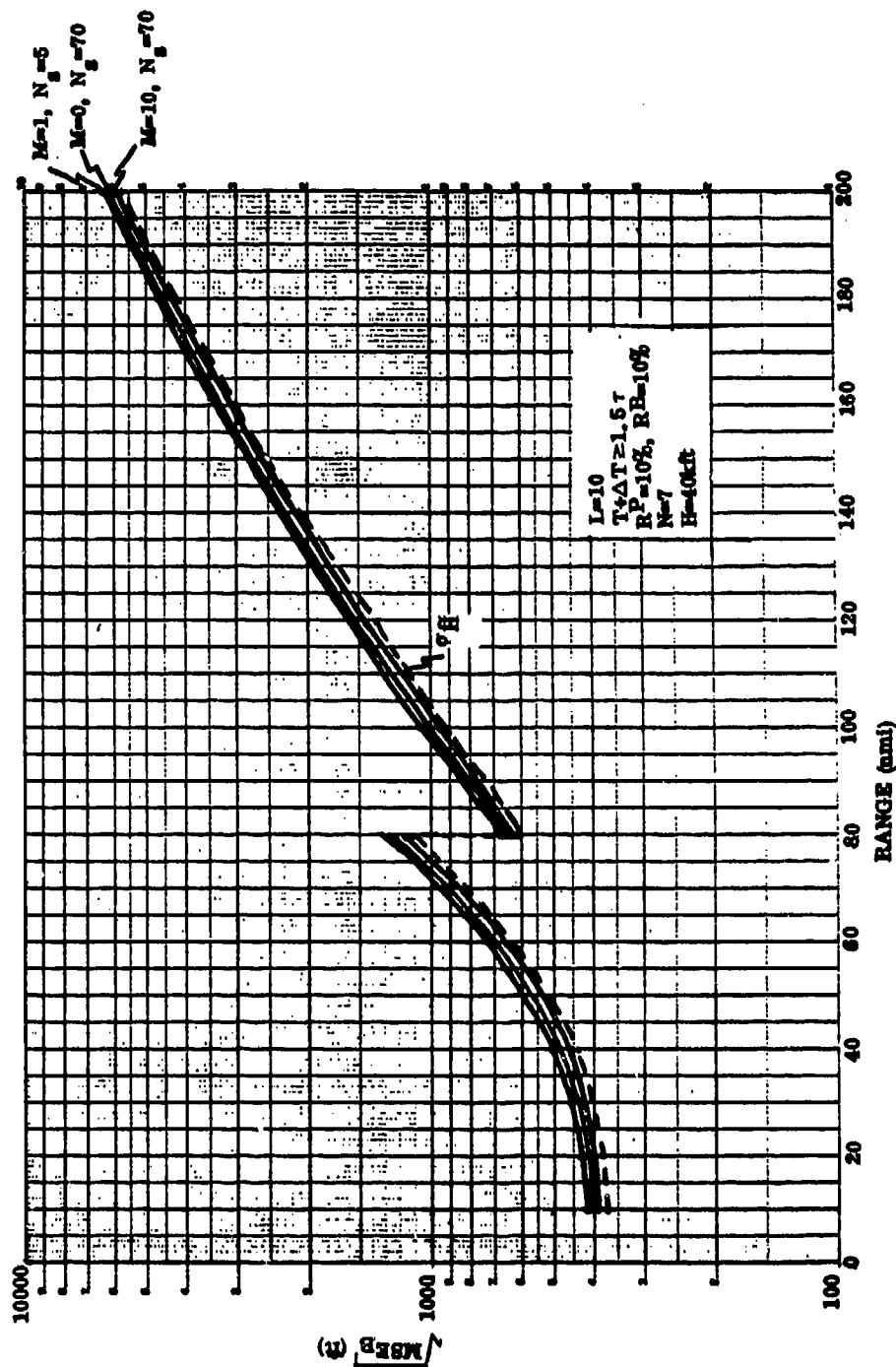


Figure 5-19. Maximum Tolerable Buyer's Limit on Total Mean Square Height Error

SECTION VI

REFERENCES

- (1) U. S. Standard Atmosphere, 1966, - U. S. Government Printing Office.
- (2) U. S. Standard Atmosphere, 1976, - NOAA - S/T 76-1562,
- U. S. Government Printing Office.
- (3) Lenhard, R. W., "Accuracy of Radiosonde Temperature and Pressure-Height Determination", Bull Amer Meterological Soc., Vol. 51 No. 9, September 1970.
- (4) Thayer, G. D.; Bean, B. R.; An Analysis of Atmospheric Refraction Errors of Phase Measuring Radio Tracking Systems Part I, NBS Report 7254, June 1962.
- (5) Abramowitz, M.; and Stegun, I. A., Handbook of Mathematical Functions, NBS Applied Mathematics Series 55, December 1965.

ENGLISH-METRIC/METRIC-ENGLISH CONVERSION TABLE

mm	=	0.1 cm	lb	=	453.6 g
cm	=	0.3937 in.	lb	=	0.4536 kg
cm	=	0.0328 ft	metric ton	=	1.12 tons (U.S.)
cm	=	10 mm	m	=	39.37 in.
cm ²	=	0.1550 in. ²	m	=	3.281 ft
cm ²	=	1.076 · 10 ⁻³ ft ²	m	=	1.0936 yd
cm ³	=	0.061 in. ³	m ²	=	10.76 ft ²
cm ³	=	3.531 · 10 ⁻⁵ ft ³	m ²	=	1.196 yd ²
ft	=	30.48 cm	m ³	=	35.32 ft ³
ft	=	0.3048 m	m ³	=	1.430 yd ³
ft ²	=	0.0929 m ²	mi	=	1.6093 km
ft ²	=	929.37 cm ²	mi	=	5280 ft
ft ²	=	9.294 · 10 ⁻³ km ²	mi	=	0.87 nmi
ft ³	=	0.0283 m ³	mi	=	1760 yd
in.	=	2.54 cm	mi ²	=	2.59 km ²
in. ²	=	6.452 cm ²	mi/h	=	0.87 knots
in. ³	=	16.387 cm ²	nmi	=	1.852 km
μm	=	0.001 mm	nmi	=	6076 ft
(micron)			nmi	=	1.15 mi
μm	=	10 ⁻⁶ m	yd	=	0.9144 m
μm	=	10 ⁻⁴ cm	yd ²	=	0.836 m ²
μin.	=	2.54 · 10 ⁻⁵ mm	yd ³	=	0.7645 m ³
kg	=	2.2046 lbs	qt	=	0.946 liter
km	=	3281 ft	liter	=	1.057 qt
km	=	0.6214 mi	acre	=	43,560 ft ²
km	=	0.55 nmi	acre	=	4046.72 m ²
km ²	=	1.076 · 10 ⁷ ft ²	rad	=	57.2958°
km ²	=	0.381 mi ²	deg	=	0.017 rad
km/h	=	0.913 ft/s	°F	=	9/5(°C) + 32
knot	=	1.152 mi/h	°C	=	5/9(F° - 32)
oz	=	28.35 g			
oz	=	0.032 lbs			